PLOS COMPUTATIONAL BIOLOGY

RESEARCH ARTICLE

Selective ion permeation involves complexation with carboxylates and lysine in a model human sodium channel

Emelie Flood, Céline Boiteux, Toby W. Allen*

School of Science, RMIT University, Melbourne, Vic, Australia

* toby.allen@rmit.edu.au

Check for updates

OPEN ACCESS

Citation: Flood E, Boiteux C, Allen TW (2018) Selective ion permeation involves complexation with carboxylates and lysine in a model human sodium channel. PLoS Comput Biol 14(9): e1006398. https://doi.org/10.1371/journal.pcbi.1006398

Editor: Alexander MacKerell, University of Maryland School of Pharmacy, UNITED STATES

Received: January 28, 2018

Accepted: July 24, 2018

Published: September 12, 2018

Copyright: © 2018 Flood et al. This is an open access article distributed under the terms of the Creative Commons Attribution License, which permits unrestricted use, distribution, and reproduction in any medium, provided the original author and source are credited.

Data Availability Statement: All relevant data are within the paper and its Supporting Information files.

Funding: We acknowledge financial support from the National Institutes of Health (Grant number U01- HL126273-01/02), https://www.nih.gov; the National Health and Medical Research Council of Australia (Grant numbers APP1104259 and APP1141974), https://www.nhmrc.gov.au; the Australian Research Council (Grant number DP170101732), http://www.arc.gov.au; the

Abstract

Bacterial and human voltage-gated sodium channels (Na_vs) exhibit similar cation selectivity, despite their distinct EEEE and DEKA selectivity filter signature sequences. Recent high-resolution structures for bacterial Na_vs have allowed us to learn about ion conduction mechanisms in these simpler homo-tetrameric channels, but our understanding of the function of their mammalian counterparts remains limited. To probe these conduction mechanisms, a model of the human $Na_v1.2$ channel has been constructed by grafting residues of its selectivity filter and external vestibular region onto the bacterial Na_vRh channel with atomic-resolution structure. Multi-μs fully atomistic simulations capture long time-scale ion and protein movements associated with the permeation of Na^+ and K^+ ions, and their differences. We observe a Na^+ ion knock-on conduction mechanism facilitated by low energy multi-carboxylate/multi-Na^+ complexes, akin to the bacterial channels. These complexes involve both the DEKA and vestibular EEDD rings, acting to draw multiple Na^+ into the selectivity filter and promote permeation. When the DEKA ring lysine is protonated, we observe that its ammonium group is actively participating in Na^+ permeation, presuming the role of another ion. It participates in the formation of a stable complex involving carboxylates that collectively bind both Na^+ and the Lys ammonium group in a high-field strength site, permitting pass-by translocation of Na^+. In contrast, multiple K^+ ion complexes with the DEKA and EEDD rings are disfavored by up to 8.3 kcal/mol, with the K^+-lysine-carboxylate complex non-existent. As a result, lysine acts as an electrostatic plug that partially blocks the flow of K^+ ions, which must instead wait for isomerization of lysine downward to clear the path for K^+ passage. These distinct mechanisms give us insight into the nature of ion conduction and selectivity in human Na_v channels, while uncovering high field strength carboxylate binding complexes that define the more general phenomenon of Na^+-selective ion transport in nature.

Author summary

Ion channels can rapidly and selectively conduct an ionic species, essential for the firing of neurons, where sodium and potassium channels respond to changes in membrane potential to release stores of sodium and potassium ions in succession. The ability of a protein

Medical Advances Without Animals Trust (Australia), http://www.mawa-trust.org.au; and supercomputing support from the Pittsburgh Supercomputing Center, DE Shaw Anton (Grant number PSCA17045P; NRBSC, through NIH RC2GM093307), https://www.psc.edu; and the National Computational Infrastructure (Australia; Grant number dd7), http://nci.org.au. The funders had no role in study design, data collection and analysis, decision to publish, or preparation of the manuscript.

Competing interests: The authors have declared that no competing interests exist.

pore to discriminate between these two nearly identical ions has remained an intriguing problem for decades. In particular, the origins of sodium selectivity have been obscured by diverse protein chemistries that exhibit sodium-selective conduction in prokaryotes and eukaryotes. Here we use multi-microsecond atomistic simulations to observe and contrast the permeation mechanisms of sodium and potassium ions in model human and bacterial sodium channels. These channels exhibit shared features of conduction, centered on the involvement of charged protein groups that form complexes with the smaller sodium ion. In the human channel model, we observe a special role for the signature lysine that allows sodium to pass, but partially blocks potassium. As sodium channels are vital to heartbeat, sensation, muscle contraction and brain activity, these insights could assist developments in improved therapeutics for disorders such as epilepsy and chronic pain, with mechanisms relevant to a range of ion transport processes in biology and materials.

Introduction

Voltage-gated sodium (Na_v) channels are widely distributed in the central and peripheral nervous systems where they participate in essential functions, including heartbeat, muscle contraction and brain activity [1, 2]. Dysfunctional Na_vs are associated with several physiological disorders, including epileptic seizures and chronic pain [3, 4], and they are therefore a major target for new drugs [5]. However, our understanding of the fundamental mechanisms governing these channels remains incomplete, largely due to the lack of high-resolution structural data on mammalian Na_vs. There have, however, been recent breakthroughs in the structural determination for several Na_v channels that enable investigations into molecular mechanisms.

The first high-resolution structure of a Na_v channel was the X-ray structure of the bacterial channel Na_vAb [6], which was followed by numerous other high resolution structures, including for Na_vRh [7], Na_vAep1 [8] and Na_vMs [9, 10]. Although no mammalian Na_v structure is yet available, two eukaryotic Na_v structures have recently been solved using cryo EM; Na_vPaS from cockroach [11] and a newly resolved $EeNa_v1.4$ from electric eel [12], released after the simulations in this study were completed. Na_vPaS has a 36–46% sequence identity to human Na_v channels, but is 300–500 residues shorter. Na_vPaS has several residues in and around the SF unresolved, has reduced charge in the vestibule of the SF compared to human Na_vs and a resolution of 3.8 Å [11]. $EeNa_v1.4$ has a 65% sequence identity to the human $Na_v1.4$ and a resolution of 4 Å [12]. The lower resolution of these structures is significant given the small size of the Na_v SF (diameter of ~3.6 Å at its narrowest point [12]), and thus while these new structures help guide and validate studies, there remains much to be learned from the existing high-resolution bacterial structures. Bacterial and human Na_v channels share several features including Na^+-selective conduction, voltage-dependent activation, pore-based inactivation and drug modulation [13–16]. While there is only a 25–30% sequence identity between bacterial and human Na_vs [10], there exists evidence for overall shared structure [13]. Human Na_vs consist of four domains, DI-DIV, linked together to form one long polypeptide chain, whereas the simpler bacterial channels are made up of four identical subunits [13] (Fig 1A). Each of these domains/subunits consists of 6 helical trans-membrane spanning segments, S1-S6, where S1-S4 make up a voltage sensor domain (VSD) and S5-S6 the pore domain (PD). Between these two latter segments is a P-loop that includes a narrow ion selectivity filter (SF) [13] (Fig 1B and 1C), which establishes an ion preference "fingerprint" (permeability $Li^+ \sim Na^+ > K^+ \sim Cs^+ \sim Rb^+$) that is the same for both bacterial and human Na_vs [1, 17, 18]. Both eukaryotic

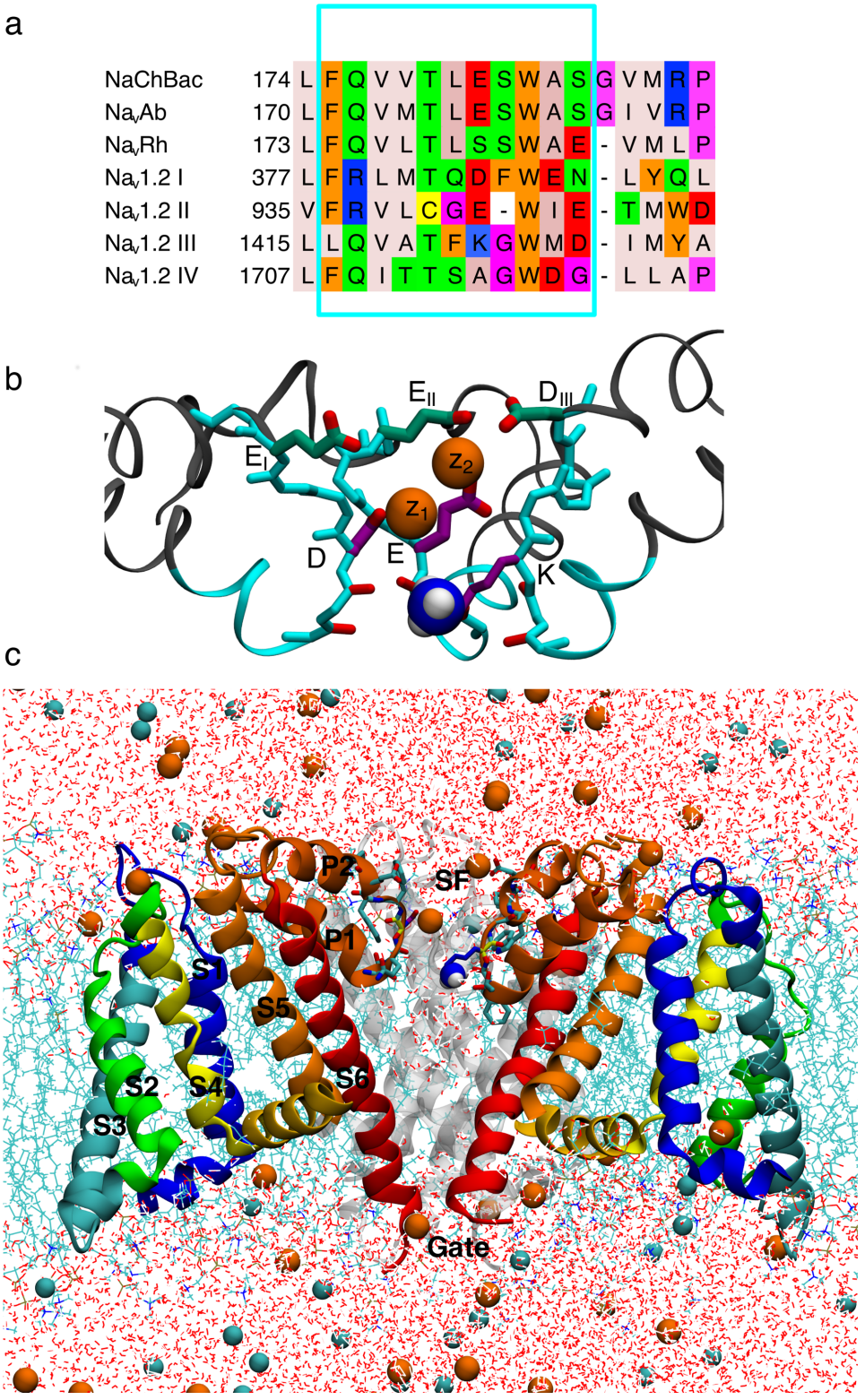

Fig 1. Human $Na_v1.2$ model ion channel system. a) Jalview [81] sequence alignment of bacterial NaChBac, Na_vAb and Na_vRh, with the four domains of human $Na_v1.2$ (labeled DI-DIV). Amino acids are colored according to their properties using the Zappo coloring scheme [81]. Cyan box selection marks the grafted $Na_v1.2$ residues. Red box selection marks the EEEE/DEKA signature sequences responsible for selectivity. b) SF and vestibule of the Na_vRh/$Na_v1.2$ model with grafted residues in cyan. The residues in the inner DEKA and outer EEDD rings are indicated in

purple and green, respectively, and the charged ammonium group of the Lys is shown as blue and white balls. c) $Na_vRh/Na_v1.2$ channel embedded in a hydrated DPPC bilayer (cyan sticks), surrounded by water (red and white sticks) with Na^+ and Cl^- ions (orange and cyan balls). Three out of four monomers are shown (front subunit removed for clarity; rear subunit in gray), with VSD in green/blue/yellow and the PD in orange/red ribbons.

https://doi.org/10.1371/journal.pcbi.1006398.g001

and bacterial Na_vs are Na^+ over K^+ selective with eukaryotic Na_vs selecting for Na^+ with P_{Na+}/P_{K+} ~10–30 [1, 19] and bacterial Na_vs with P_{Na+}/P_{K+} ~5–170 [17, 18, 20]. Due to the structural and functional similarities, the bacterial Na_v channels offer an excellent template, or scaffold, to support investigation into the core functional activities of mammalian Na_vs.

Despite overall conservation of structure and function, the channels present distinct SF sequences (Fig 1A), with bacterial Na_v channels making use of a ring of four Glu side chains (EEEE), to create a high field strength binding site (S_{HFS}) thought to favor Na^+ [13], whereas all mammalian Na_v utilize a ring of Glu, Asp, Lys and Ala (DEKA; Fig 1A) [13, 19, 21], containing not only acidic residues, but also a basic lysine side chain that is known to be crucial to selectivity in mammalian channels [19, 21]. So how do these different channels achieve similar ion selectivity, and does the existence of disparate sequences mean that bacterial and mammalian channels impose their ion preference via different molecular strategies [18]? We seek to reveal and compare the fundamental rules of selective ion permeation for the whole family of sodium channels, by exploring ion conduction mechanisms in a human Na_v channel to compare to previous simulations in bacterial channels.

There are 9 different Na_vs comprising $Na_v1.1$ to $Na_v1.9$ [22], with highly conserved sequences throughout these different subtypes [23]. $Na_v1.2$ is abundant in the human nervous system and has been investigated extensively using methods of mutagenesis and electrophysiology (e.g. [21, 24, 25]). Here we take advantage of the conserved structural and functional features between mammalian and bacterial channels to generate a model of $Na_v1.2$, which incorporates the key SF and vestibular regions, into a high-resolution bacterial structure. Such grafting has previously been successful experimentally for imparting Ca^{2+} selectivity on a bacterial Na_v channel [26]. The bacterial Na_vRh structure was chosen as the scaffold due to its higher sequence similarity in and around the SF (Fig 1A; only shown for Na_vAb, Na_vRh and $Na_v1.2$, however, it can be seen that the same is true also for Na_vMs, Na_vAe and Na_vCt [16]). In particular, other bacterial Na_vs have one residue extra just above the SF (Gly182; Na_vAb numbering) compared to $Na_v1.2$ (Fig 1A). Furthermore, those channels have an arginine (Arg185; Na_vAb numbering) close to the SF that was found to interfere with the side chains of the $Na_v1.2$ SF in our separate models using Na_vAb as a scaffold (not shown). We also note that proposed open structures of a bacterial Na_v have been presented [9, 16, 27], but our simulations (not reported here) have suggested that the proposed open Na_vMs structure does not stay open without strong constraints, as discovered previously [28]. Furthermore, previous studies of ion selectivity in bacterial Na_vs using a closed lower gate have shown good sampling of ion translocation throughout the SF [18, 29–31], and are thus capable of shedding light on selectivity mechanisms by revealing the underlying equilibrium free energy surfaces governing multi-ion movements. There is minimal thermodynamic perturbation for ions in the SF and cavity due to the closed lower gate, with the free energy of an ion inside open and closed Na_vAb pores having been shown to be similar [27].

Previous simulations of bacterial channels have taught us much about the potential behavior of the human sodium channel. The bacterial SF contains a highly conserved ring of four Glu side chains forming a high field strength site (S_{HFS}) [6]. Early simulation studies revealed ion binding sites and indications of a multi-ion conduction mechanism [28, 31–36]. These studies suggested favoring of a partly-hydrated Na^+ due to the SF geometry in the Na_vAb

crystal structure and the strength of interaction of ions with glutamate side chains [28, 31, 36]. They also demonstrated the ability of the SF to bind 2 ions concurrently within the S_{HFS} site, with higher affinity for Na^+ potentially creating a reduced permeation barrier [36]. Simulations have shown that the SF is flexible and wide enough to house multiple Na^+ ions [37], and is occupied by an average of two to three ions [29, 30, 38]; although simulations under significant membrane potentials have indicated reduced occupancy [28]. However, microsecond-length MD simulations have shown that the symmetric arrangement of Glu side chains in the crystal structure is broken on long time scales, affecting ion occupancy and having significant implications for the permeation mechanism [29, 30, 36, 39]. These studies demonstrated that there is coupling between ion translocation and SF conformation, with isomerization of glutamate side chains catalyzing Na^+ conduction. These long unbiased simulations have described a stable 2-ion state, where the ions are trapped [30]. While some studies have focused only on this 2-ion state [31, 36], it has been shown that it is when a third ion enters the SF that efficient knock-on of the bottom ion into the central cavity occurs [18, 29, 30]. The top ion can either knock-on or pass-by the middle ion in S_{HFS}, with both permeation pathways experiencing similar energy barriers (S2 Fig; [30]). Regardless, binding of Na^+ to the S_{HFS} Glu side chains is central to understanding Na^+ over K^+ selectivity [18, 30, 31, 36].

Conduction is reliant on the flexibility of these side chains [29, 30, 36], where Na^+ ions form favorable 2 ion-2 carboxylate clusters (see S2 Fig, states C_2 and C_3) that are not stable for K^+ [30]. Human Na_v channels do not possess a symmetric E ring, but contain a set of carboxylates that might mediate similar complex formation. In particular, the DEKA signature sequence (Fig 1, right inset) contains two carboxylates that may be sufficient. However, human channels also possess a well-conserved [24] charged ring in the outer vestibule, immediately adjacent to the SF, consisting of Glu, Glu, Asp and Asp residues ($E_IE_{II}D_{III}D_{IV}$; with the exception of $Na_v1.7$ that contains $E_IE_{II}I_{III}D_{IV}$) [40]. The residues in these two rings have been shown to be asymmetrical in position [41] and highly flexible [42], and thus may facilitate multi-ion conduction, akin to the bacterial channels.

Substitution experiments have shown that the DEKA-ring is crucial for the selection of Na^+ ions in mammalian Na_v channels [19, 21, 25], with at least one of the D and E necessary to preserve selectivity [19]. The most important carboxylate in the DEKA ring is the E, which together with the K (residue 1422 in human $Na_v1.2$), maintains wildtype (WT) selectivity, despite mutation of the D [19]. However, if the positions of these two residues (E and K) are swapped, into DKEA, selectivity is reduced nearly 4-fold [25], showing the importance of their precise locations, potentially due to interactions with surrounding amino acids, or implying a specific coordinating complex for Na^+ during conduction. Mutagenesis has also shown that both the charge and length of the K_{1422} are necessary for maintaining Na^+ selectivity; substitution of Lys with neutral side chains causing a complete loss of Na^+ selectivity, and substitution with negatively charged side chains even reversing selectivity [19]. Previous computational studies examining the role of Lys in conduction have also been based on models using bacterial structures, and concluded on a passive blocking role for Lys. Xia et al. replaced the ring of four Ser in the bacterial channel Na_vRh with DEKA and performed MD simulations to find that only when the Lys was constrained to E_{IV} was the SF permeable to Na^+ and K^+ ions [43, 44]. Mahdavi et al. threaded the amino acids from rat $Na_v1.4$ onto the backbone of a pore only model of Na_vAb, also suggesting that ion translocation requires displacement of Lys out of the permeation pathway, by hydrogen bonding to the neighboring DIV Ser [45]. We will show in this study, using extended length simulations, that Lys in fact plays an active role in conduction (not just based on pore occlusion) that is quite different for Na^+ and K^+ ions.

The vestibular EEDD-ring has also been shown to be important for ion conduction, possibly because it increases the electrostatic attraction of extracellular cations [24, 25, 46, 47].

However, all four residues are not equally important, with cysteine mutations showing the greatest decrease in conduction occurs when domain II Glu is mutated (effect on conduction: $E_{II}>E_I> D_{IV}\sim D_{III}$) [25, 41]. Furthermore, mutagenesis experiments have shown that replacement of EEDD residues can be detrimental to Na^+ selectivity. In particular P_{Na}/P_K has been shown to decrease when D_{IV} is replaced with Cys [40, 41, 48], while other experiments have shown little or no effect [25, 49]. Functionally, therefore, the exact roles of the outer ring carboxylates in selectivity are not well defined. Previous models based on bacterial structures have implied a greater thermodynamic preference for Na^+ in the lower SF, and an additional outer binding site at the EEDD-ring [43, 45]. However, we will show that on long timescales, SF rearrangements allow for stable complexes with carboxylates from both the S_{HFS} and outer ring that are important to Na^+ permeation.

Experiments have suggested that Na_vs possess multiple binding sites inside the SF [50–53]. However, the evidence for their ability to bind multiple ions at the same time is inconclusive [50–55]. Investigations of flux coupling suggest a flux ratio exponent close to unity for mammalian Na_v channels, which is generally thought to imply a 1-ion conduction mechanism [51, 54, 55]. Furthermore, anomalous mole fraction effects, considered evidence of ion cooperation during conduction, have only been observed in bacterial [18] and not mammalian Na_vs [53]. Such effects are normally expected in single-file channels that impose ion correlation [56], but may also arise from preferential and localized ion binding [57–59]. Single-file conduction is unlikely in Na_v channels given their size [60] and flexibility [42]. However, absence of an anomalous mole fraction effect does not rule out ion cooperativity. The fact that anomalous mole fraction effects are seen in bacterial Na_v channels in the absence of bona fide single-file permeation, as suggested by several simulation studies, as well as the decoupling of ion and water fluxes [28], demonstrates limitations in the ability of this measure to identify a multi-ion mechanism. Likewise, there exists contradictory evidence from single channel conductance measurements for mammalian Na_v channels, which have shown a saturating dependence on concentration in some experiments, indicative of a single ion mechanism [50–52], whereas others, where a wider range of concentrations have been examined, witness a complex relationship that may be explained by a multi-ion conduction mechanism [53]. Thus the experimental evidence is inconclusive when it comes to the ion occupancy and potential multi-ion conduction mechanism in mammalian Na_vs. Molecular dynamics (MD) simulations can therefore help us elucidate the mechanisms involved in ion selectivity in Na_vs.

Bacterial and human Na_v channels therefore both possess several carboxylate side chains in (or adjacent to) the SF, allowing for multiple high field strength sites that may bind one or more ions, possibly leading to increased Na^+ selectivity [61]. In a multi-ion/multi-ligand complex there will be competition between favorable ion-ligand and unfavorable ligand-ligand and ion-ion energies [62], needing long time scale simulations to capture the ion and protein configurations [29, 30]. The mechanism is further complicated by the presence of the Lys, which may increase the sampling challenges due to side chain isomerizations. We thus turn to long MD simulations to capture those ion and slowly interconverting protein movements using the DE Shaw Anton supercomputer. We have performed multi-μs simulations where Na^+ and K^+ are permitted to freely diffuse into and out of the SF of the Na_vRh/Na_v1.2 model, observing the involvement of DEKA and outer EEDD rings, as well as participation of the signature Lys in multi-ion binding complexes, revealing distinct permeation mechanisms for Na^+ and K^+ ions.

Methods

We have created a model of human Na_v1.2 that includes the most important residues for ion permeation and selectivity, using a structurally well-defined bacterial channel as a scaffold.

Although other parts of the channel may be important for attracting ions [11], the main functional region involves the SF and outer vestibular regions [24]. The sequence alignment in Fig 1 was used to create a model of human $Na_v1.2$ based on the bacterial Na_vRh structure (PDB:4DXW [7]), due to their higher sequence homology in and around the SF region, as discussed above. The mutated region (framed in cyan in Fig 1A), spanning residues 174–184 (Na_vRh numbering used herein), was chosen to introduce the SF and vestibular sequence with minimal perturbation. This includes the human DEKA and EEDD rings (residues 180 and 183/184) in the upper SF. Furthermore, residues 174–177 are located behind the SF and may interact with the side chains of the SF. In particular, within that range is Na_vRh Q175, which is a positively charged Arg in $Na_v1.2$ DI and DII, and may influence both structure and ion conduction. To minimize perturbation, side chains of the chosen amino acids were removed from Na_vRh and the corresponding $Na_v1.2$ side chains rebuilt manually using the CHARMM program [63]. Herein the residues from the DEKA ring will be referred to by their 1-letter abbreviations. To avoid confusion with the symbol for Lys (K), potassium will always be referred to in ionic form, K^+. The Asp and Glu residues from the vestibular EEDD ring will be referred to according to their domain numbers (E_I, E_{II}, D_{III} and D_{IV}).

Between the DEKA ring and the EEDD ring the $Na_v1.2$ sequence is one residue shorter in DII than in the bacterial channels. This residue (number 181) was removed, and neighboring residues (180–182) joined with constrained MD simulation (see below). We note that the original Na_vRh SF structure was closed at the lower gate as well as having a slightly collapsed SF. The collapsed SF has been proposed to be associated with the orientation of the Ser181 side chains, blocking the SF [64], however, after removing the Ser side chains as well as patching $Na_v1.2$ residues and equilibration (described below), the filter forms an open SF conformation that allows us to study ion permeation (Fig 1B and 1C). Other changes to the model, including the rebuilding of missing intracellular loops connecting S2 and S3 helices in the VSD using Rosetta [65], and the maintenance of a key hydrogen bond between Thr178 and Trp182 that has been postulated to be important for keeping the shape of the SF in bacterial Na_v [6, 7], are described in the Supplementary Information.

It is difficult to predict or measure the pK_a shift of Lys in a non-aqueous microenvironment with the coming and going of conducting ions, such as in the SF of a Na_v channel [66]. Large pK_a shifts have been recorded in channel environments, and protonation states depend on the exact environment and ion occupancy, which will fluctuate over time [67]. The dependence of Na_v conduction on the protonation states of key residues in the SF has therefore been investigated in several studies of bacterial Na_vs [30, 36, 68]. Furthermore, quantum mechanical calculations using simplified models of the DEKA ring alone have demonstrated that a thermodynamic preference for Na^+ may be achieved with either protonation state of the Lys [61]. However, the signature Lys has been shown to be crucial to Na^+ selectivity [19], intuitively suggesting that its charge may be important. To cover both possibilities, we have examined Na^+ ion movements with both charged and neutral lysine, which will help us isolate the role of that charge in ion conduction.

The proteins were embedded in lipid bilayers of dipalmitoyl-phosphatidylcholine (DPPC), being the best characterized lipid for MD simulations [69], with explicit TIP3P water molecules [70] and 150 mM of NaCl or KCl solution. Systems were built and pre-equilibrated with CHARMM [71] and further equilibrated using NAMD [72] prior to unbiased production simulations carried out on the purpose-built supercomputer Anton [73, 74] for 4 μs for Na_vRh/$Na_v1.2$ with charged Lys both for NaCl and KCl, and 2 μs for neutral Lys (less time required due to better sampling of ion movements), totaling 10 μs. Simulations all used the CHARMM36 [69] lipid and CHARMM22 protein and ion parameters [72] with CMAP corrections [75], chosen to provide direct comparison to our past simulations of the bacterial

Na_vAb channel [30]. However, attention to ion-carboxylate parameters was given to ensure accurate interactions for Na^+ and K^+ inside the SF, with standard parameters for the ion-carboxylate interaction shown to lead to reasonable agreement with both *ab initio* MD free energies of binding and osmotic pressure data [76]. Descriptions of both ion-carboxylate and corrected ion-carbonyl interactions are discussed in the Supplementary Information.

The free energy map, or potential of mean force (PMF), for ion movement was calculated for each system using trajectory data with specific pore ion occupancies, from unbiased simulations as $W(\{z_i\}) = -k_BT \ln \rho(\{z_i\}) + C$, where ρ is the unbiased probability distribution as a function of reaction coordinate(s) $\{z_i\}$, being the vertical positions of one or more ions (z_1, z_2, or z_3; defined with z_1 being the lower-most ion), or their centroids (e.g. $z_{12} = (z_1 + z_2)/2$), each relative to the center of mass of the protein, z_{ref}, and where C is a constant. See Supplementary Information for more details, including error calculations.

The most important states involved in the permeation of Na^+ and K^+ ions across the SF were identified from the PMFs and cluster analysis. The frames were broken down according to ion occupancy as well as ion-ion and ion-carboxylate distances (S1 Table). Different states were identified according to how many carboxylates were interacting with the ion/ions using a cutoff defined from the radial distribution functions in S3 Fig, with further details of the clustering method described in the Supplementary Information. These states include complexes involving one or more carboxylate groups, Na^+ or K^+ ions and/or the signature Lys ammonium group. To evaluate the relative binding affinities of these states, Free Energy Perturbation (FEP) [77] calculations were performed to obtain the relative binding free energies of Na^+ and K^+ to each particular complex. Details of these, and other calculations, including structural comparisons of available X-ray and Cryo-Em structures, and continuum electrostatic calculations to examine ion-binding propensities, are provided in the Supplementary Information.

Results and discussion

A stable human Na_v model with asymmetric and flexible selectivity filter

After patching of $Na_v1.2$ SF and vestibular residues into the bacterial channel, followed by equilibration, the overall structures of the PD and SF were stable and settled down to RMSD 2–3 Å (S4 Fig) after initial changes during the first μs of simulation, with the level dependent on the choice of Lys protonation state (see below). Late changes are seen, especially for simulations in KCl, due to the onset of permeation following conformational changes within the SF, described below. The first 1 μs of the $Na_v1.2$ model with charged Lys with NaCl and KCl and the first 0.25 μs of the shorter simulation with uncharged Lys have been discarded as equilibration (S5 Fig). We observe that the $Na_v1.2$ SF is relaxing into an asymmetrical shape where the DEKA and EEDD-ring span ~10–15 Å, allowing interactions with residues other than their immediate neighbors (S5 Fig), explaining the increased RMSD. Previous experiments involving cysteine mutations have shown that the residues in the filter of an Na_v channel are indeed asymmetrical in height and that the inner and outer rings span up to ~15 Å [41]. This asymmetry destabilizes the Thr/Cys178-Trp182 bond, important for keeping the shape of the SF in bacterial channels [6, 7], which are seen to break and form several times during the simulations.

Flexibility has been shown to be a critical property of the bacterial Na_v channel SF to facilitate ion conduction [29, 30]. Furthermore, pairwise cysteine mutations have suggested significant flexibility (up to 7 Å) of the residues in the SF of a mammalian Na_v [48] [42]. We observe high flexibility in the $Na_vRh/Na_v1.2$ SF (S6 Fig, with mean SF backbone fluctuations being approximately twice as large as those for Na_vAb (RMSF~1.5 Å and RMSF~0.8 Å for $Na_vRh/Na_v1.2$ and Na_vAb, respectively) (S6A and S6B Fig). These RMSF values (S6A Fig) are mostly

due to asymmetric subunit movements, with the RMSF values halved when computed based on subunit-by-subunit orienting (S6B Fig).

The recent eukaryotic Na_vPaS [11] and $EeNa_v1.4$ [12] cryo EM structures offer related structural data to validate our model, although at limited resolution where several SF side chains were not resolved, preventing immediate conclusions about specific interactions. Structural alignment between the $Na_vRh/Na_v1.2$ model and the Na_vPaS or $EeNa_v1.4$ structures (S1 Fig) shows structural similarities between the proteins, with key residues at the same positions. Due to the highly dynamic nature of the SF and its side chains, structural comparisons are limited and will depend on the choice of structure from the model simulation. Overall, however, structures are consistent, with the RMSD of the SF and vestibular region (residue 178 to 184) backbone being 2.0 Å and 2.3 Å when aligning to all four subunits (S1A Fig), and 1.8 Å and 2.1 Å when aligning subunit by subunit (S1A Fig), for Na_vPaS and $EeNa_v1.4$, respectively. The residues of the DEKA and EEQD/EEDD rings are asymmetrical in position in all three structures, with these residues spanning 10–15 Å in the model, ~10 Å in Na_vPaS and ~14 Å in $EeNa_v1.4$ (S1 Fig). The spread of these side chains in both our model and the Na_vPaS and $EeNa_v1.4$ structures, combined with the high flexibility and lack of experimental resolution in this region, indicates that SF dynamics may play an important role in conduction.

Selectivity filter with neutral lysine exhibits bacterial-like multi-ion complex formation and conduction

The DEKA Lys has been shown to be crucial to Na^+ selectivity in mammalian Na_v channels [19]. However, the protonation states of amino acids in a dynamic microenvironment, like that seen here within the SF), are hard to pinpoint experimentally [66] and may have large fluctuations [67]. We have therefore investigated ion permeation in $Na_v1.2$ not only with a protonated (Lys^+) but first also with a deprotonated Lys (Lys^0). Importantly, this allows us to isolate the role that the positive charge may play in the SF of $Na_v1.2$ for Na^+ permeation, and offers a comparison to existing bacterial Na_v simulations.

Permeation of Na^+ in the SF of the $Na_v1.2$ model when its DEKA Lys is neutral involves both 2-ion and 3-ion conduction mechanisms with an average number of 2.1±0.2 Na^+ ions in the SF, similar to (albeit slightly less than, though within the errors) that seen in the bacterial channel Na_vAb (2.3±0.5 ions; [30]). The ions are partly hydrated as they permeate the SF (S7 Fig). In the time series for ion movements shown in Fig 2, several ions (colored lines) are observed to enter and exit the central cavity (below −5 Å), often coexisting within the SF (S1 Movie). We see 61 complete permeation events through the SF (inward or outward moving involving 16 distinct ions) and the ions appear to move independently of the neutral Lys side chain (black line). Snapshots in Fig 2 show representative configurations of a 2-ion and 3-ion state, where we see multi Na^+-ion/multi-carboxylate complexes similar to those in for the bacterial Na_v ([30]; see also Fig 3E and 3F, to be discussed below). However, in the $Na_v1.2$ channel it most commonly not only involves carboxylates only from the inner DEKA-ring, but also from the outer EEDD-ring, whose carboxylates reach down to help coordinate the ions, as opposed to only using two carboxylates from the inner ring, as was the case of the bacterial Na_vAb channel [30].

This cooperation between the DEKA and EEDD-rings creates a longer SF binding region with a broad span of negative electrostatic potential (Fig 3A and 3B), leading to less distinct binding sites. While Na_vAb has all of its charged side chains in one symmetrical ring, $Na_v1.2$ has its charges spread out in two asymmetrical and highly flexible rings creating a broad S_{HFS} (ion density map shown in Fig 3C), compared to Na_vAb (Fig 3D). Commonly a binding site is created with two Na^+ and one or two carboxylates from the DEKA and EEDD rings (S1 Table;

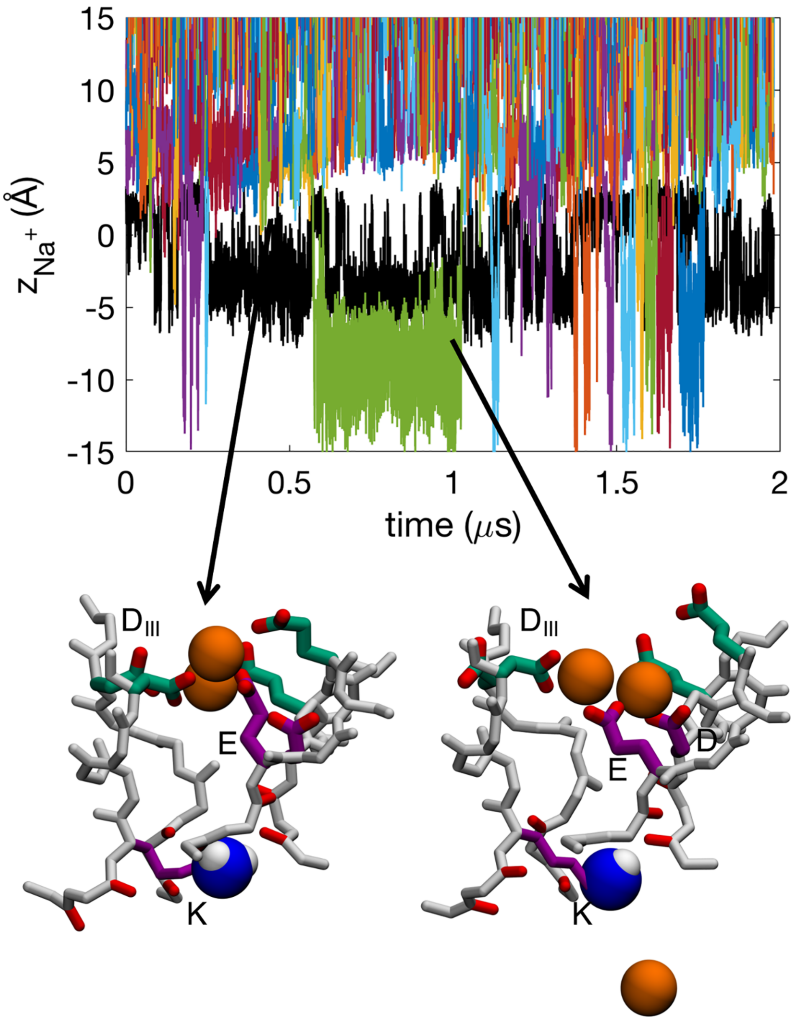

Fig 2. Time series showing the *z* positions of deprotonated Lys^0 (K; black) and Na^+ ions (colors) in the $Na_v1.2$ SF. Insets show snapshots of Na^+ ions (orange balls) in representative configurations with active residues from the DEKA (purple) and EEDD (green) rings labeled. The neutral amine group of the Lys shown is shown as blue and white balls. See also sample trajectory in **S1** Movie.

https://doi.org/10.1371/journal.pcbi.1006398.g002

column 2 and S8 Fig). The specific residues involved vary and we see several distinct carboxylate-ion complexes forming during the simulation (S1 Table; column 2 and S8 Fig).

Double ion occupancy dominates in the SF, but 3-ion occupancy is also common (S8A Fig). When the SF is occupied by a single ion it is most commonly unbound, however, it is also likely to be bound to one or more carboxylate side chains (S8B Fig). When there are two ions in the filter they most likely form single ion complexes with multiple carboxylates (S8C Fig). They are also often singly bound or bound together in a tight multi-ion/multi-carboxylate complex (defined by the radial distribution function in S3 Fig; with ions within 4.7 Å of each other and 2 or more carboxylate groups (based on central C atom) from the DEKA and EEDD-rings within 3.8 Å of the ions). When there are three ions in the SF, two of these are most likely to be bound together in a tight multi-carboxylate complex (S8D Fig). We have previously shown that multi-ion/multi-carboxylate complexes play a role in Na^+ selectivity in acid sensing ion channels [76]. When these complexes are present, the ions are mostly bound by E and/or D from the DEKA ring, together with the outer ring D_{III} (S1 Table; column 2). This

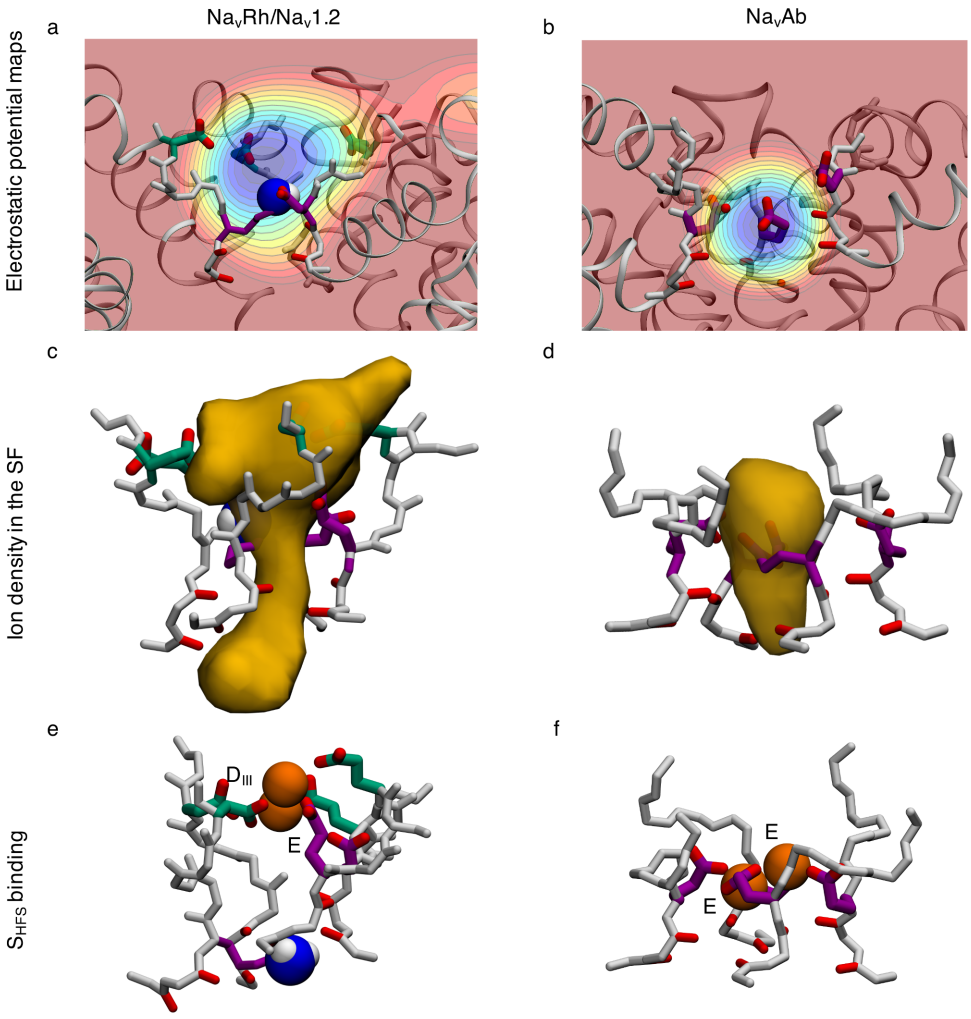

Fig 3. Comparison of electrostatic potential maps. Electrostatic maps of a) the $Na_v1.2$ SF with deprotonated Lys^0, compared to b) bacterial Na_vAb. Each contour represents 10 kcal/mol/Å/e. Density maps of Na^+ occupancy in c) the $Na_v1.2$ SF with Lys^0 and d) Na_vAb. Multi ion-multi carboxylate binding sites in e) $Na_v1.2$ and f) Na_vAb. The residues in the inner DEKA and outer EEDD rings are indicated in purple and green, respectively, and the uncharged amine group of the Lys is shown as blue and white balls.

https://doi.org/10.1371/journal.pcbi.1006398.g003

cooperativity of inner and outer charge rings is common and while all carboxylate side chains from either of the two rings ring are not necessary, at least one is needed for Na^+ binding in the S_{HFS}. In particular, the DEKA ring is involved ~80% of the time, the EEDD ring ~80% of the time, and both rings cooperatively involved ~60% of the time. This need for only one of the carboxylates in the DEKA ring to maintain cation permeability has previously been implicated by mutagenesis experiments [19].

Despite the longer SF binding region in $Na_v1.2$ with neutral Lys, we see a conduction mechanism resembling that of the bacterial Na_v, relying on multi ion-multi carboxylate clusters for an efficient knock-on conduction. When there are 2 ions within the SF, at z_1 (lower) and z_2 (upper), the free energy map (as function of z_1 and z_2) in Fig 4A exhibits three states; A_2, B_2 and C_2. In state A_2, the upper ion is in the vestibular region of the SF (z_2~14Å) and the lower ion is collectively bound by the inner (purple side chains) and outer rings (green side chains) (z_1~7Å). In state B_2 the top ion has joined the bottom ion and they are both bound by the

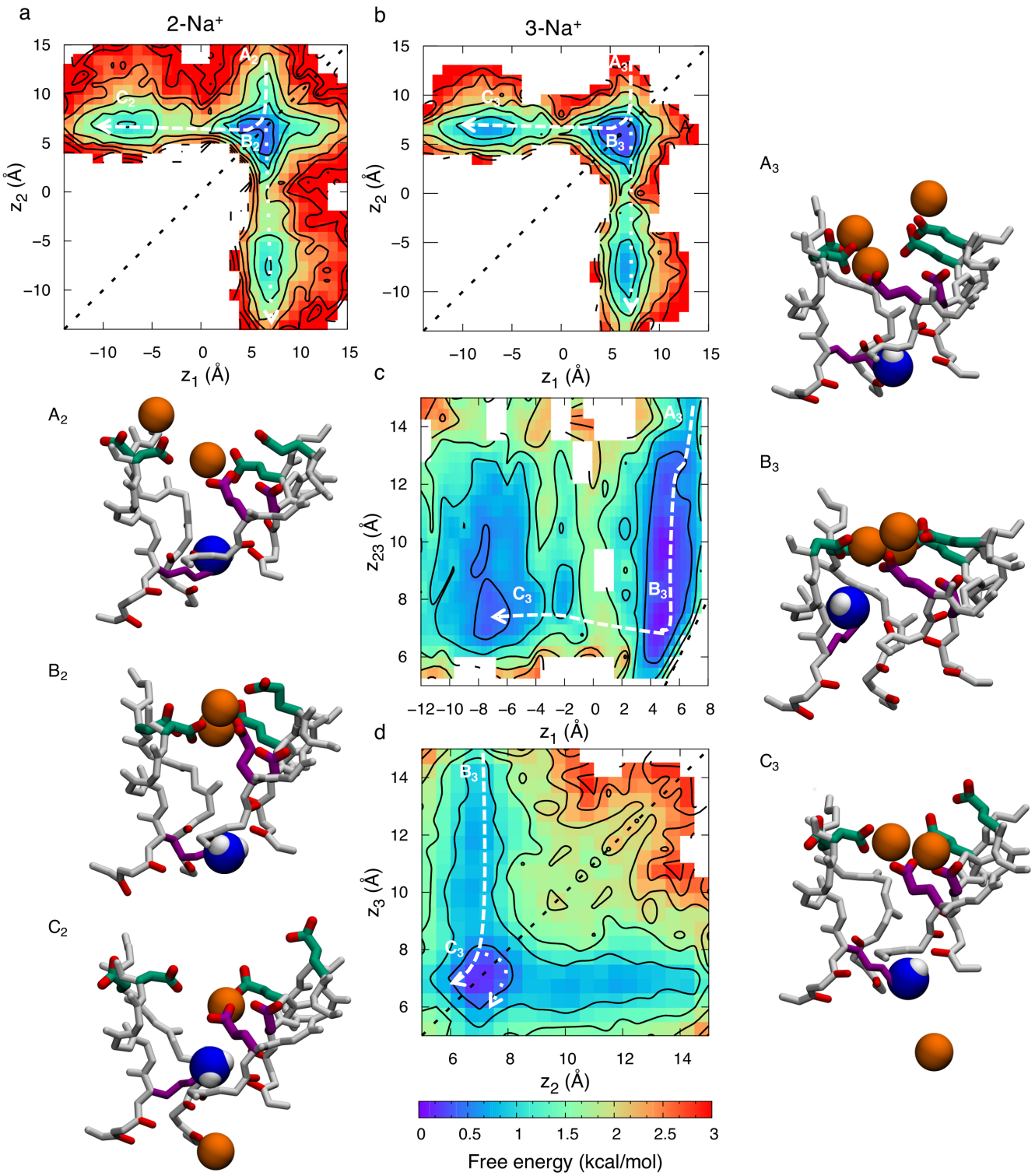

Fig 4. Permeation of Na^+ in the $Na_v1.2$ SF with deprotonated Lys^0. 2D free energy projections showing a) 2-ion conduction mechanism, and b, c & d) 3-ion conduction mechanism (graphed for the two bottom ions in b, all three ions in c, and the two top ions in d); where z_1, z_2, and z_3 correspond to the z positions of the bottom, middle and top ions, respectively, and where z_{23} is the z position of the COM of the top two ions. Each contour represents 0.5 kcal/mol. Snapshots, with the inner DEKA ring in purple, the outer EEDD-ring in green, and the uncharged amine group of the Lys shown as blue and white balls, indicate the corresponding Na^+ ion (orange ball) movements. State labels (A-D) include a subscript 2 or 3, representing the 2-ion or 3-ion mechanisms, respectively.

https://doi.org/10.1371/journal.pcbi.1006398.g004

inner and outer rings (z_1~z_2~7Å) forming cooperative tight multi-ion/multi-carboxylate clusters, commonly made up by D, E and D_{III}, and reminiscent of those seen in the bacterial Na_v (compare Fig 3E and 3F). In state C_2 the top ion has either pushed the bottom ion into the cavity by Coulomb repulsion (dashed line) or it has passed by the bottom ion and entered the cavity itself (dotted line crossing the diagonal, y = x, represented by black dashed line), in both cases translocating from z_2~7 Å to z_2~-10 Å, while the other ion remains collectively bound to the inner and outer rings. These distinct permeation pathways are equally likely, with the largest barrier encountered being 1.9±0.8 kcal/mol.

Fig 4B–4D show free energy projections for the 3-ion occupancy state, with ion positions specified as z_1 (lower ion), z_2 (middle ion), z_3 (upper ion) or z_{23} (COM of the two upper ions). Here state A_3 has one ion in the middle of the two rings (z_1~7 Å) and one ion in the vestibule (z_2~14 Å), and an additional ion entering from the bulk above (z_3~15 Å). In Fig 4B and 4C we see how the upper ion pushes the middle ion downward to bind together with the lower ion at the inner ring (z_1~z_2~6 Å), represented by state B_3, before eventually entering this site itself and pushing the bottom ion into the cavity, state C_3, completing the conduction event. The broad free energy surface in panel c is due to the range of binding sites offered by the inner and outer carboxylate rings, as well as the fact that the centroid of 2 ions may span a wide range. Fig 4D shows another projection involving only the top two ions (z_2 and z_3). The dashed line in Fig 4D shows how the top ion moves from state B_3 to state C_3 by entering the S_{HFS} and knocking the bottom ion downward. The dotted line shows an alternative path where the top ion instead passes by the middle ion before knocking the bottom ion into the cavity. Regardless of the permeation pathway, the largest barrier experienced during permeation through the SF in the 3-ion state is 1.4±0.6 kcal/mol, similar to that experienced for Na^+ in the bacterial channel (S2 Fig). These results demonstrate that low barrier conduction may occur via knock-on or pass-by mechanisms in either 2- or 3-ion occupancy states for $Na_v1.2$, but where 3-ion conduction is energetically more favorable, with reduced activation barrier. However, considering a 2-ion occupancy is more common (S8 Fig), the 2-ion mechanism is likely also contributing significantly to the overall ion flux.

We therefore have observed that the mammalian SF conducts Na^+ ions well with a neutral/deprotonated Lys in the DEKA ring, providing a useful comparison to the bacterial channel, with similar multi-ion/multi-carboxylate complexes forming during permeation (although involving both SF DEKA and vestibular EEDD carboxylates). However, because Lys is so important to permeation and selectivity experimentally [19, 21, 25], but when neutral apparently plays only a passive role that would not implicate it, this suggests that we must turn our attention to the protonated Lys case.

Charged lysine forms a high field-strength complex to facilitate Na^+ conduction

When Lys is charged, there is an average of 1.5±0.4 Na^+ ions in the SF and permeation involves either 1 or 2-ion conduction (S2 Movie). This reduction in ion occupancy (compared to the neutral Lys case above and the bacterial channel) is presumed to be due to the reduced negative charge inside the SF. If the ammonium group of the Lys was considered as another ion, we would have, in total, a similar ion occupancy of 2–3 ions in the SF. (n.b. Lys^+ may be considered another ion, as Na_v channels conduct ammonium ions nearly as well as Na^+, with relative permeability P_{NH4+}/P_{Na+} = 0.16 [60]). The time series in Fig 5 reveals that several ions (colored lines) enter and leave the SF, but it is not until the second half of the 4 μs simulation that ions begin to cross the charged Lys and enter the cavity beneath, after which we observe 28 complete permeation events (defined as any ion crossing downward or upward past the Lys, and involving 6 distinct ions that experience repeat crossings).

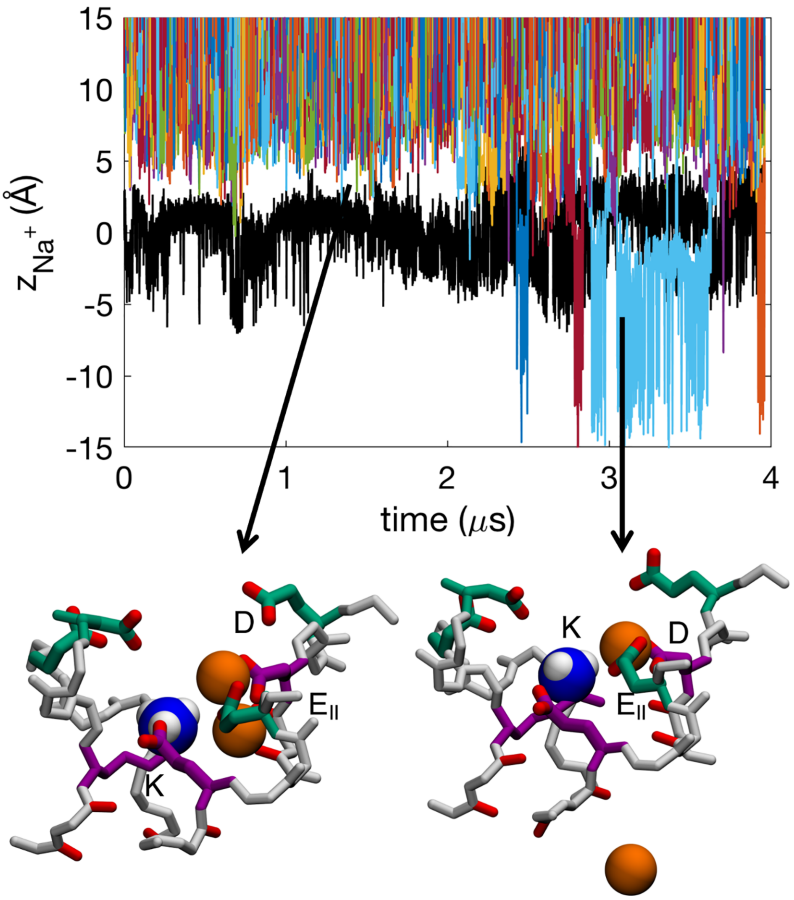

Fig 5. Time series of *z* positions for protonated Lys^+ (K; black) and Na^+ ions (colors) in the $Na_v1.2$ SF. Insets show snapshots of Na^+ ions (orange balls) in representative configurations with active residues from the inner DEKA (purple) and outer EEDD (green) rings labeled. The charged ammonium group of the Lys is shown as blue and white balls. See also sample trajectory in **S2** Movie.

https://doi.org/10.1371/journal.pcbi.1006398.g005

Snapshots in Fig 5 show representative configurations of 1- and 2-ion carboxylate complexes. As with the neutral Lys case, we see multi-ion/multi-carboxylate complex formation where the residues from the EEDD ring (green) bend down into the SF region, leading to the binding of ions together with the carboxylates from the DEKA ring (purple; see also S1 Table; column 3). The DEKA ring is involved in binding ~50% of the time, the EEDD-ring ~90% of the time, and both rings cooperatively involved ~40% of the time. These complexes are most commonly (69±11%) involving D from DEKA and E_{II} from EEDD. The ammonium group of the Lys from DEKA is also involved, binding 61±10% of the time to the E or D from the DEKA-ring. The salt bridge between Lys and one or both of these residues has previously been suggested by mutagenesis experiments as being important for Na^+ selectivity [19], and may be responsible for the importance of the precise sequence position of the Lys in the DEKA ring [25]. We also observe that when ions enter the SF, the ammonium group of Lys (black line in Fig 5) is displaced downward; being knocked-on, like any other ion. Thus, the charged Lys is intimately involved in the multi-ion mechanism. Importantly, it also participates in a Lys $+Na^+$/carboxylate complex, similar to the 2-ion/multi-carboxylate clusters, commonly coordinated by D and E_{II} and sometimes additionally by E (S1 Table; column 5). The ability to form these complexes is likely dependent on the location of the Glu and Lys in the DEKA ring, and

swapping their positions might affect this complex formation thus decreasing selectivity, as indicated by mutagenesis experiments [25]. We will see below how this tight cluster plays an important role in the conduction mechanism.

Free energy projections reveal the relationship between the ions and the position of the ammonium group of Lys, z_{Lys}, demonstrating conduction with 1-ion and 2-ion occupancies in the SF. When there is a lone ion in the SF, at z_1, the free energy map (as function of z_1 and z_{Lys}) in Fig 6 exhibits four states; A_1, B_1, C_1 and D_1. In state A_1, the ion is in the outer vestibular region of the SF (z_1~14Å) and the Lys is bound to one of the inner ring carboxylates (z_{Lys}~1 Å). In state B_1, the ion has entered deeper into the SF and is bound to the inner and outer rings (z_1~6 Å). The dotted line shows an alternative state, B_1', in which the ion entering the filter replaces the ammonium group of the Lys, which is displaced downward (from z_1~6 Å & z_{Lys}~1 Å to z_1~4 Å & z_{Lys}~-2 Å). It is interesting to note that there is no conduction occurring when this happens. The ion is bound tightly to the DEKA ring and the ammonium group of the Lys is too repulsive for it to pass by in the lower part of the filter, where the electrostatic potential is not as negative. However, the dashed line shows how the ion can cross the ammonium group of the Lys in a region of higher field strength created by multiple carboxylates (z~2 Å), leading to state C_1. In state C_1 the ammonium group of the Lys remains bound to the inner ring (z_{Lys}~2 Å) and the ion is bound to the backbone carbonyl of the two residues underneath the DEKA ring (z_1~-2 Å). In state D_1 the ion has left the SF and entered the cavity (z_1~-8 Å), completing the permeation event. The dashed arrow shows the minimum free energy path for conduction, where the largest barrier encountered is 1.7±0.3 kcal/mol.

The 2-ion conduction mechanism is summarized in Fig 7. The free energy projection in Fig 7A shows the position of the bottom ion (z_1) as a function of the Lys (z_{Lys}), Fig 7B shows the COM of the two ions (z_{12}) as a function of the Lys, while Fig 7C shows bottom versus top ions. In this 2-ion case, we see five distinct states; state A_2 is like the corresponding 1-ion state A_1, but with an additional ion entering from the bulk above (z_{12}~14 Å). In Fig 7B we can see how the two ions enter deeper into the SF and bind collectively to the inner and outer rings, just above the Lys in state B_2 (z_1~z_2~7 Å & z_{Lys}~2 Å). There is an additional state B_2', related to B_2, where the ammonium group of the Lys is displaced downward (from z_1~6 Å & z_{Lys}~2 Å to z_1~4 Å & z_{Lys}~-2 Å; dotted line). However, just as for the 1-ion state, this downward Lys displacement is not sufficient for conduction, instead requiring that the ammonium group of Lys rise up and join one of the ions in a new intermediate stable state C_2 as shown in Fig 7A (z_1~z_{Lys}~2 Å). This state only appears when there are 2 Na^+ ions in the filter and seems to be vital for efficient permeation, because it allows the ion to pass the Lys with reduced energetic barrier (dashed line). The ion then binds below the Lys to the backbone carbonyls of the lower SF represented by state D_2 (z_1~-2 Å & z_{Lys}~2 Å). In state E_2 the top ion pushes the bottom ion into the cavity and binds to the inner ring (z_1~-6 Å, z_2~6 Å & z_{Lys}~2 Å). Fig 7C shows only the two ions, at z_1 (lower) and z_2 (upper), and the corresponding states. The top ion can either enter and knock on or pass by the bottom ion. The dashed arrows show the lowest free energy path for conduction. The greatest barrier to overcome in the 2-ion state is 1.6±0.7 kcal/mol. Importantly, while conduction was seen to be possible with a singly-occupied SF (seen in Fig 6; dashed line), the entrance of a second Na^+ ion enables a stable state (Fig 7A; state C_2) where the ammonium group of the Lys and the bottom ion are collectively bound by the carboxylates, this allows the ion to pass by the Lys and in to the cavity with a lower barrier. As we shall see below, this efficient conduction mechanism does not exist for K^+ ions.

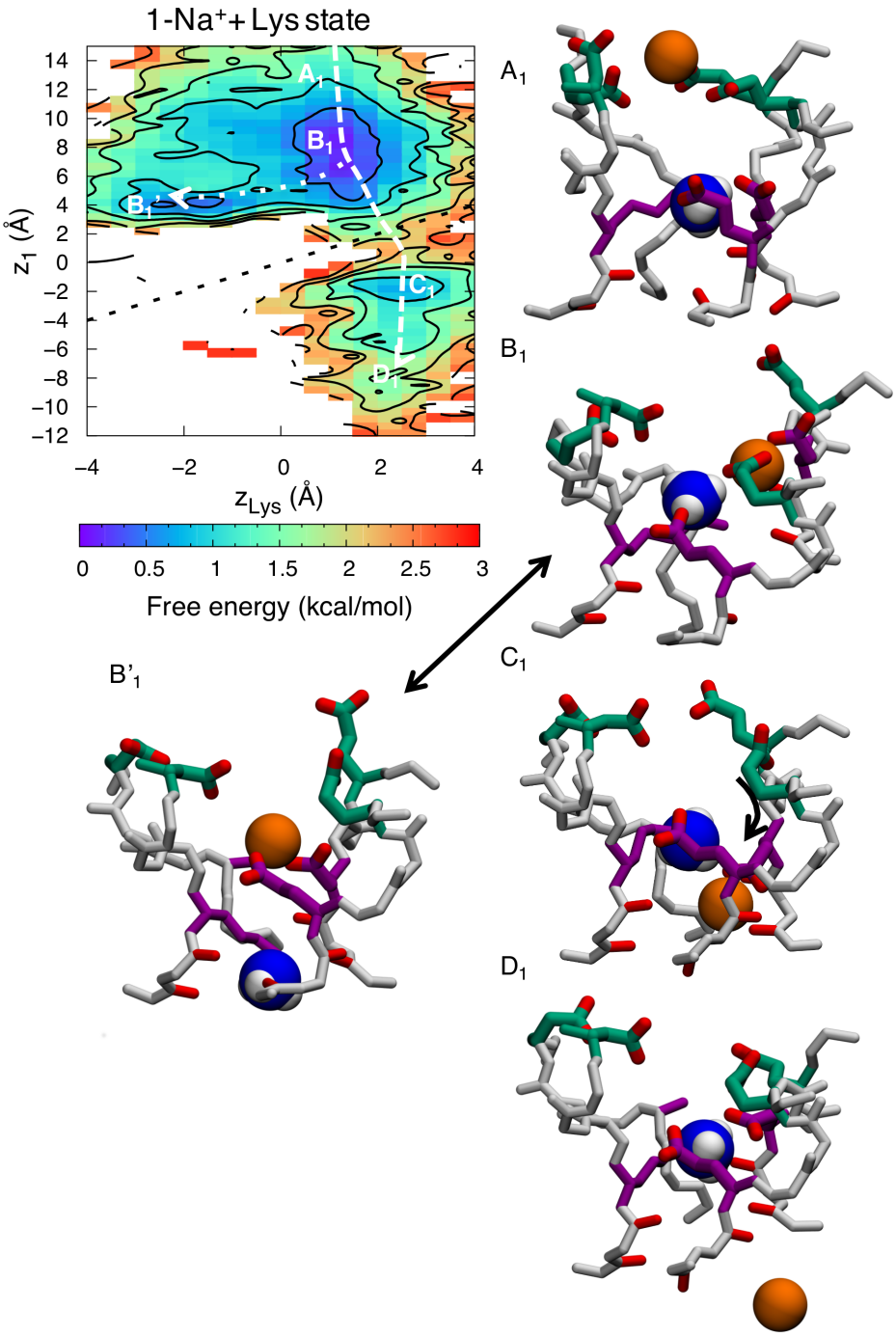

Fig 6. Single ion permeation for Na^+ in the $Na_v1.2$ SF with protonated Lys^+. 2D free energy projections showing 1-ion conduction mechanism where z_1 corresponds to the z position of the ion and z_{Lys} the z position of the Lys^+ ammonium group. Snapshots, with the inner DEKA ring in purple, the EEDD ring in green and the charged ammonium group of the Lys shown as blue and white balls, indicate the corresponding Na^+ ion (orange balls) movements.

https://doi.org/10.1371/journal.pcbi.1006398.g006

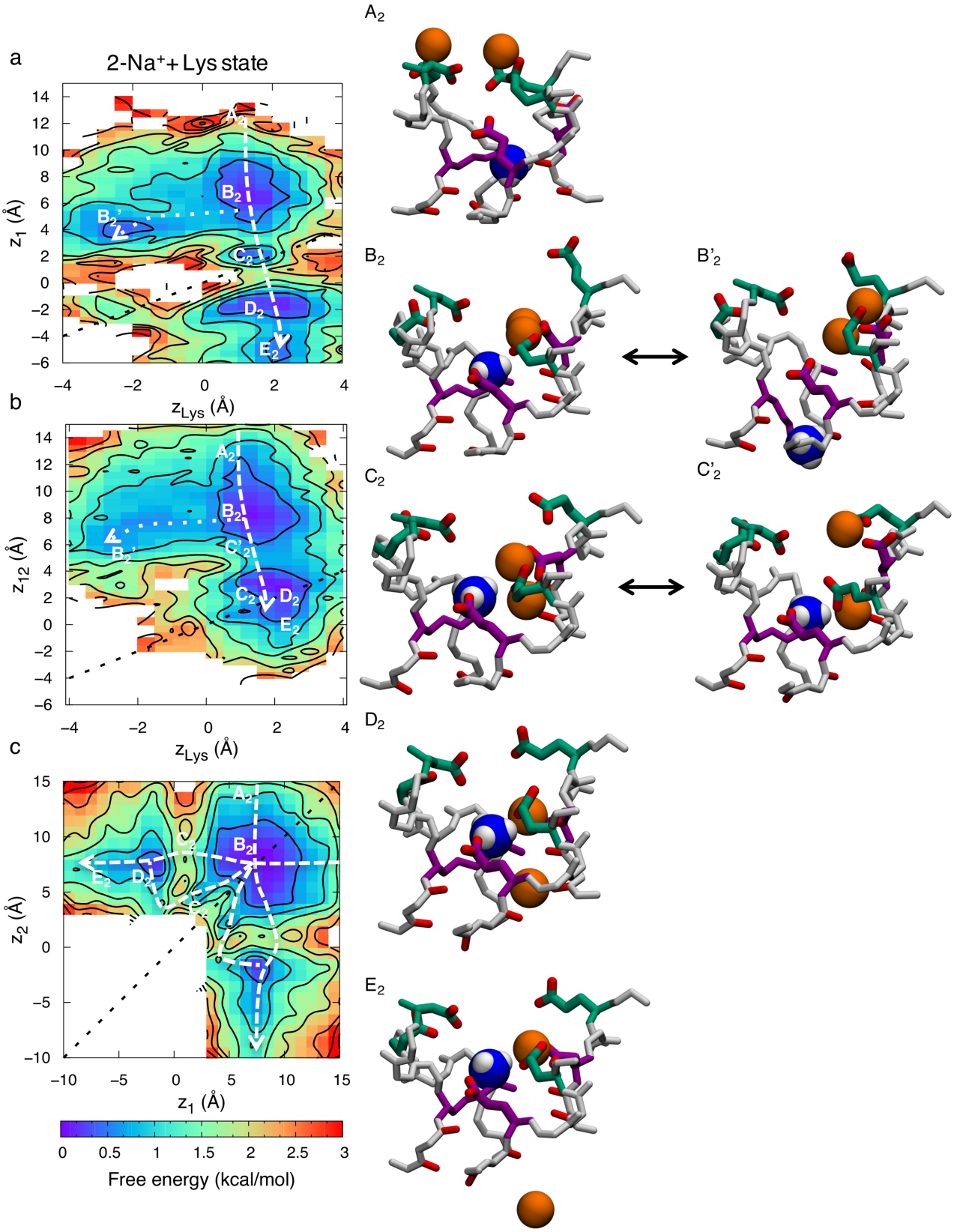
a
2-Na+ + Lys state
z1 (Å)
zLys (Å)
b
z12 (Å)
zLys (Å)
c
z2 (Å)
z1 (Å)
Free energy (kcal/mol)
A2
B2
B'2
C2
C'2
D2
E2

Fig 7. Two-ion permeation for Na^+ in the $Na_v1.2$ SF with protonated Lys^+. 2D free energy projections showing the 2-ion conduction mechanism for: a) the bottom ion and Lys; b) the two ions and Lys; and c) the two ions; where z_1 and z_2 correspond to the z positions of the bottom and top ions, z_{12} the z position of the COM of the two ions, and z_{Lys} the z position of the Lys^+ ammonium group. Snapshots, with the DEKA ring in purple, EEDD ring in green, and the charged ammonium group of the Lys shown as blue and white balls, indicate the Na^+ ion (orange balls) movements.

https://doi.org/10.1371/journal.pcbi.1006398.g007

K^+ exhibits less multi-ion complex formation, and is partially blocked by lysine

The $Na_v1.2$ SF with charged Lys, in the presence of KCl solution, has an average occupancy of 1.3±0.1 K^+ ions, being slightly lower than for Na^+ ions, but comparable within errors. Fig 8 shows several ions (colored lines) entering and exiting the SF but not interacting extensively with the Lys (black line). We see 38 complete K^+ ion permeation events (involving 13 distinct ions with repeat crossings, predominantly in the latter half of the 4 μs simulation after Lys rotamer change; see below and S3 Movie), being similar but somewhat less than the Na^+ case above.

Most of the time there exists a single K^+ ion in the SF (S9 Fig). When there are two K^+ ions in the SF they are generally further from each other, with a mean ion-ion distance of 15.1±0.8 Å, compared to 11.4±1.2 Å for Na^+. Snapshots in Fig 8 show representative configurations. The K^+ ions most commonly bind to single carboxylates or stay unbound (S9 Fig). The lower occupancy and the larger ion-ion distances mean that we do not see the same tight multi-ion/multi-carboxylate complexes as frequently as we did for Na^+ (S9 Fig), and when they do occur they are almost always singly coordinated by outer ring carboxylates (S1 Table; column 4). Instead, a single K^+ ion typically enters the SF and binds solely to the D from the DEKA ring (S1 Table; column 6). The DEKA ring is involved in binding ~40% of the time, the EEDD ring ~70% of the time, and both rings cooperatively involved only ~10% of the time. This reduced binding and absence of complex formation deep in the SF slows K^+ permeation. We instead observe K^+ ions held bound to the D of DEKA, electrostatically repelled by the Lys ammonium group, until the Lys side chain changes rotamer downward to allow ion movement, in stark contrast to the Na^+ case above.

We again see conduction with either 1 or 2 K^+ ion occupancy. However, unlike for Na^+ ions, we see similar permeation mechanisms when 1 or 2 K^+ ions are in the SF. This, together with the large K^+- K^+ distance of 15.1±0.8 Å, compared to 11.4±1.2 Å for Na^+, suggest that the second ion does not participate in conduction but rather is loosely associated around the vestibule region. Fig 9A shows the 1-ion conduction mechanism, with the ion at z_1, and the ammonium group of Lys, at z_{Lys}. We observe four states in the 2D PMF in Fig 9; A_1, B_1, C_1 and D_1. In state A_1 the ion is in the vestibular region of the SF (z_1~14 Å) and the Lys is bound to one of the inner ring carboxylates (z_1~0 Å). The ion then moves down and binds to the outer ring (z_1~8 Å) represented by state B_1. In state C_1, the ion has entered deeper into the SF and is now bound only to the carboxylate of the D_1 from the DEKA ring (z_1~4 Å). The Lys is still bound to the inner ring in both these two states (z_K~0 Å). The ions do not have considerable effect on the position of the ammonium group of the Lys. However, occasionally (~10% of the time) the Lys changes rotamer downward (z_{Lys}<-2 Å), allowing leakage of K^+ ions and thus permeation, represented by dashed line, leading to state D_1. After the conduction event, the ammonium group of the Lys again bends upward to bind to the inner ring carboxylates (z_{Lys}~2 Å). For this to happen the K^+ ion has to pass by the ammonium group of the Lys in the lower part of the SF (z_1~z_{Lys}~-2 Å) where the electrostatic potential is less negative, leading to a larger energy barrier of 2.8±0.3 kcal/mol, as seen in Fig 8A along the pathway represented with a dashed arrow. This increased barrier (by 1.1±0.4 kcal/mol) would suggest a relative permeability for the channel of the order of 10, which is consistent with the experimental value for mammalian Na_v

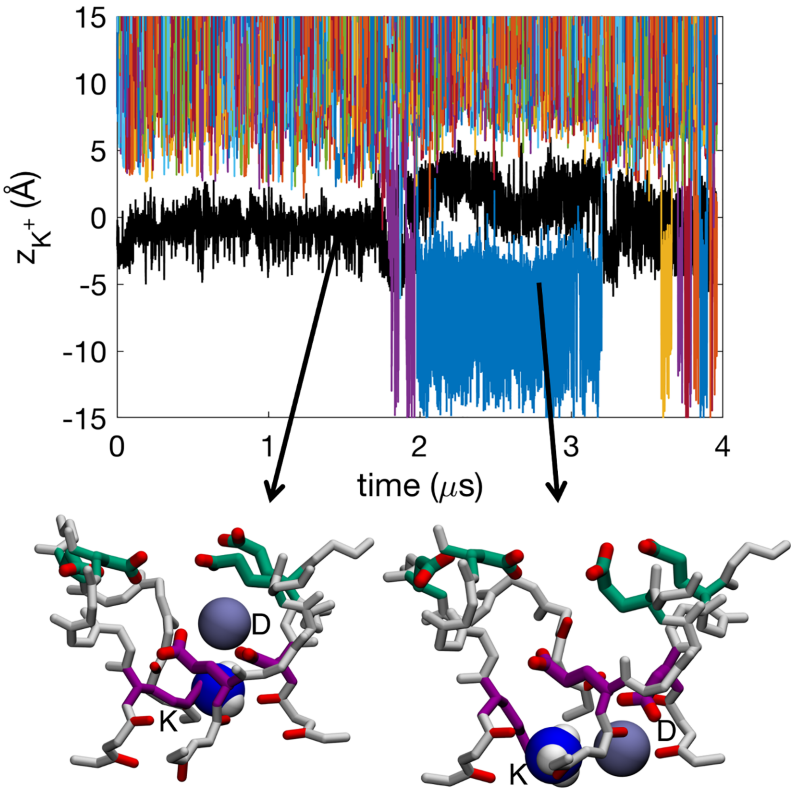

Fig 8. Time series of *z* positions for protonated Lys$^+$ (K; black) and K$^+$ ions (colors) in the SF of Na$_v$1.2. Insets show snapshots of K$^+$ ions (purple balls) in representative configurations with active residues from the DEKA (purple) and EEDD (green) rings labeled. The label for the Lys of DEKA, "K", should not be confused with the potassium ion K$^+$. The charged ammonium group of the Lys shown is shown as blue and white balls. See also sample trajectory in S3 Movie.

https://doi.org/10.1371/journal.pcbi.1006398.g008

channels (e.g. P_{Na+}/P_{K+} ~10 in Na$_v$1.2 from rat [25]). This estimate, however, assumes the rate-limiting step for conduction does not involve Lys rotameric change, which was observed here on the multi-μs timeframe; apparently exceeding the sub-μs scale of permeation, but which may not have been reliably quantified based on 4μs simulation.

The 2-ion conduction mechanism in Fig 9B looks very similar, with the large K$^+$- K$^+$ distance of 15.1±0.8 Å showing that it is the same as the 1-ion conduction mechanism, only with an additional ion in the vicinity. Fig 9B shows the 2D PMF with the bottom ion, at z_1, and the ammonium group of Lys, at z_{Lys}, being almost identical to the 1-ion case in Fig 9A; supporting the lack of a concerted 2-ion conduction mechanism. The lower ion enters the channel, binds collectively to the DEKA and EEDD rings in state B_2, before binding solely to the DEKA ring in state C_2. To enter the cavity, the ion has to wait for the Lys to change rotamer, it can then pass the Lys ammonium group in the lower SF, and then move further down into the cavity (state D_2). In the meanwhile, the upper ion generally sits in the vicinity of the SF. In Fig 9C we see how the two ions can cross each other in the top part of the channel. The top ion can be anywhere between z_2~7 Å and z_2~15 Å during conduction, however, with a slight preference around z_2~12 Å. The 2-ion energy barrier is similar to the 1-ion case at 2.7±0.3 kcal/mol. The Na$^+$ and K$^+$ barriers differ by 1.1 kcal/mol, however, the slowest coordinate in the K$^+$ translocation pathway appears to involve the structural isomerization of the Lys side chain downward to permit conduction, leading to a permeation event that is more costly for K$^+$.

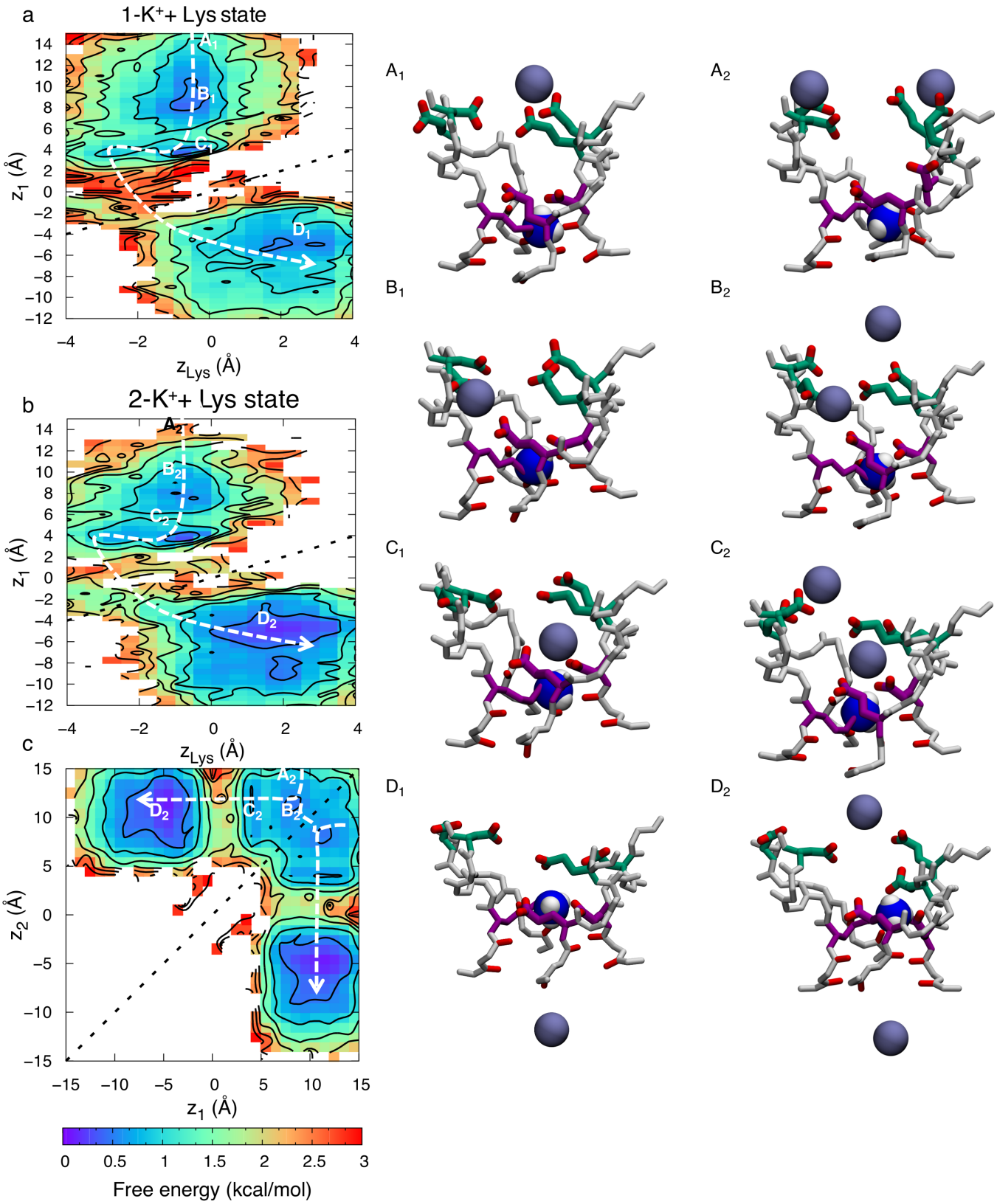

Fig 9. Permeation of K^+ in the $Na_v1.2$ SF with protonated Lys^+. 2D free energy projections showing: a) 1- ion conduction mechanism; b & c) the 2-ion conduction mechanisms (graphed for the bottom ion and Lys in b, and the two ions and Lys in c); where z_1 corresponds to the z position of the bottom ion, z_2

the z position of the top ion, and z_{Lys} the z position of the Lys/K ammonium group. Snapshots for 1-ion (left) and 2-ion (right) mechanisms, with the DEKA ring in purple, EEDD ring in green, and the charged ammonium group of the Lys shown as blue and white balls, indicate K^+ ion (purple balls) movements. State labels include a subscript 1 or 2, representing the 1-ion or 2-ion mechanisms, respectively.

https://doi.org/10.1371/journal.pcbi.1006398.g009

Key to the low barrier for Na^+ permeation is its ability to form tight multi-ion/multi-carboxylate clusters as well as a complex with Lys and 2 carboxylates, allowing pass-by conduction in the S_{HFS}. We do not see the same tight K^+-K^+ clusters nor the simultaneous binding of K^+ and Lys near the DEKA ring. Instead we see a lone K^+ ion that is singly bound and forced to pass by the Lys lower in the SF (S9 Fig), where the electrostatic field is less favorable (Fig 3A), making the whole process far less likely.

We now explore the thermodynamic stabilities of the complexes observed during permeation events to understand the causes of the different Na^+ and K^+ mechanisms that may underlie selectivity.

Multi-ion complex stability underpins selective conduction

Multi-ion complex formation with carboxylates is required for efficient permeation as it helps draw in and stabilize the ions in the SF. This acts as a precursor for the ion+Lys/multi-carboxylate complex that aids in the crossing of the SF. The analysis in S9 Fig suggests that such multi-ion/multi-carboxylate complexes appear more favorable for Na^+ over K^+. When the SF is occupied by a single ion, Na^+ is most commonly bound to one or more carboxylate side chains (45% and 26%), whereas K^+ is more likely to be unbound (61%) (S9B Fig), and Na^+ is several times more likely than K^+ to form multi-carboxylate complexes (26% vs. 6%). Of the multi-ion occupancies observed, Na^+ ions are most likely to be either singly bound or in loose multi-carboxylate complexes (42% and 40%), whereas K^+ is most likely to be either singly bound or unbound (52% and 36%). Na^+ is several times more likely to form tight multi-ion/multi-carboxylate clusters than K^+ (12% vs. 3%) (S9C Fig). For Na^+ ions, these clusters are predominantly made up by outer ring carboxylates together with either the E or D from the DEKA ring, most commonly E_{II} together with D (S1 Table; column 3). For K^+ such complexes are almost always made up only by the outer ring carboxylates (S1 Table; column 4).

Thus, tight 2-ion/multi-carboxylate complexes, similar to the complex that is formed before the low free energy pass-by conduction events for Na^+ (Fig 7; state B_2), are more common for Na^+ than K^+, and may be very important for selectivity (S9 Fig). FEP calculations were used to investigate the relative stabilities of Na^+ and K^+ in such a complex. The most representative multi-ion/multi-carboxylate complex was identified to be bound collectively by D and E_{II} (Fig 10B and 10C; inset) (69%) (S1 Table; column 3). Results from FEP calculations show preferential binding by Na^+ with 4.8±0.1 kcal/mol for single ion occupancy (Fig 10A), showing a strong inherent preference by carboxylates to bind Na^+, in agreement with Eisenman high field strength theory on ion selectivity [78]. Quantum mechanical calculations using a model DEKA ring have demonstrated a similar preference for Na^+ over K^+ (4.8 kcal/mol [79]), revealing consistency between models. The same complex containing two ions shows a large preference of 8.3±0.1 kcal/mol for Na^+ over K^+ ions (Fig 10B and 10C); 4.2 kcal/mol from the transformation of the 1st ion (Fig 10B) and 4.1 kcal/mol from the transformation the 2nd ion (Fig 10C). This shows that an additional ion creates extra stability for Na^+ relative to K^+. When another ion is added to the complex, the cumulative ion-carboxylate attraction increases faster than the carboxylate-carboxylate and ion-ion repulsion, more so for Na^+ than K^+, giving additional stability to Na^+ complexes. These complexes create deeper binding in the SF that aids crossing the ammonium group of the Lys. We note that this large cumulative free energy difference between Na^+ and K^+ ions to form a 2-ion complex with multiple carboxylates is not

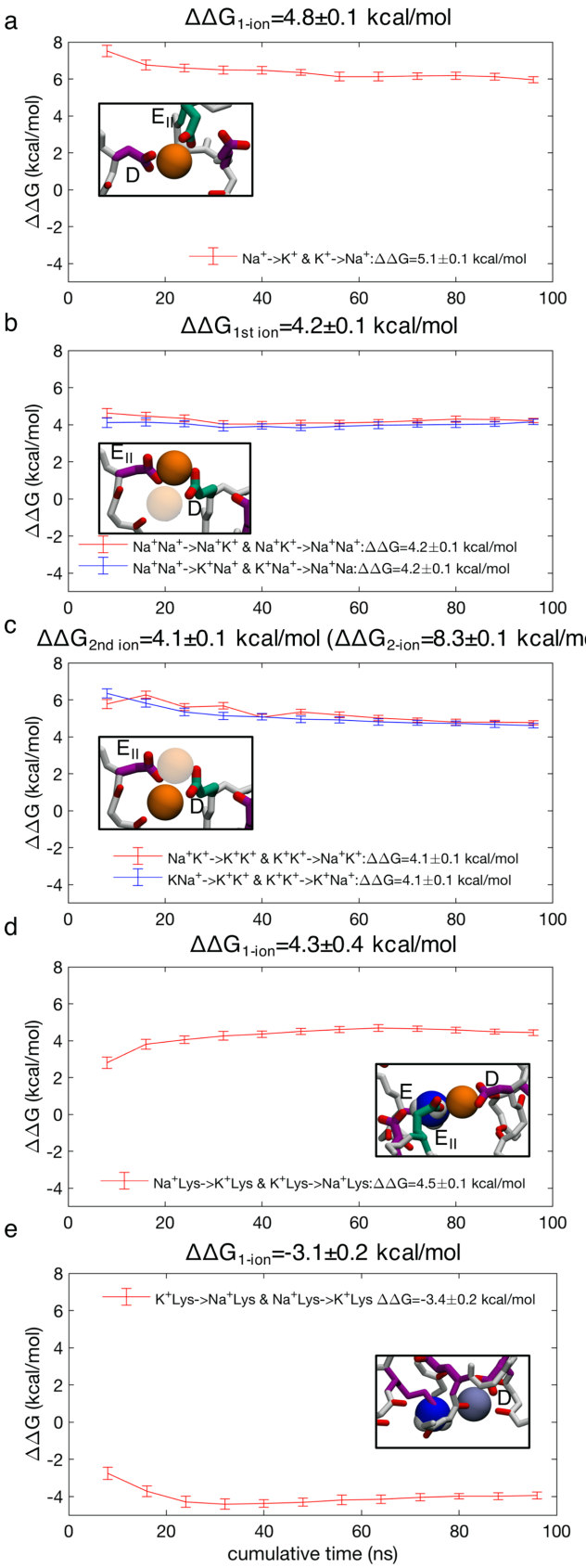
a
ΔΔG1-ion=4.8±0.1 kcal/mol
ΔΔG (kcal/mol)
EII
D
Na+->K+ & K+->Na+:ΔΔG=5.1±0.1 kcal/mol
b
ΔΔG1st ion=4.2±0.1 kcal/mol
ΔΔG (kcal/mol)
EII
D
Na+Na+->Na+K+ & Na+K+->Na+Na+:ΔΔG=4.2±0.1 kcal/mol
Na+Na+->K+Na+ & K+Na+->Na+Na:ΔΔG=4.2±0.1 kcal/mol
c
ΔΔG2nd ion=4.1±0.1 kcal/mol (ΔΔG2-ion=8.3±0.1 kcal/mol)
ΔΔG (kcal/mol)
EII
D
Na+K+->K+K+ & K+K+->Na+K+:ΔΔG=4.1±0.1 kcal/mol
KNa+->K+K+ & K+K+->K+Na+:ΔΔG=4.1±0.1 kcal/mol
d
ΔΔG1-ion=4.3±0.4 kcal/mol
ΔΔG (kcal/mol)
E
D
EII
Na+Lys->K+Lys & K+Lys->Na+Lys:ΔΔG=4.5±0.1 kcal/mol
e
ΔΔG1-ion=-3.1±0.2 kcal/mol
ΔΔG (kcal/mol)
K+Lys->Na+Lys & Na+Lys->K+Lys ΔΔG=-3.4±0.2 kcal/mol
D
cumulative time (ns)

Fig 10. Free energy perturbation for ion binding selectivity. a) Single ion $Na^+ \rightarrow K^+$ and $K^+ \rightarrow Na^+$ in an ion-DE_{II} complex; b) 1st ion transformations $Na^+Na^+ \rightarrow K^+Na^+$, $Na^+Na^+ \rightarrow Na^+K^+$, $K^+K^+ \rightarrow K^+Na^+$ and $K^+K^+ \rightarrow Na^+K^+$ in the 2-ion-DE_{II} complex (with 2nd ion grayed out) and c) 2nd ion transformations $K^+Na^+ \rightarrow K^+K^+$, $Na^+K^+ \rightarrow K^+K^+$, $K^+Na^+ \rightarrow Na^+Na^+$ and $Na^+K^+ \rightarrow Na^+Na^+$ (bottom) in the 2-ion-DE_{II} complex (with 1st ion grayed out). d) single ion transformations $Na^+ \rightarrow K^+$ and $K^+ \rightarrow Na^+$ for the ion+Lys-DEE_{II} complex; e) single ion transformations $K^+ \rightarrow Na^+$ and $Na^+ \rightarrow K^+$ in an ion+Lys position in the lower SF (note that K^++Lys is the starting configuration in this case, leading to a negative free energy corresponding to the transformation $K^+ \rightarrow Na^+$). The value for the bulk reference for $Na^+ \rightarrow K^+$ in aqueous solution was found to be 17.7 ± 0.3 kcal/mol. Insets show starting configurations and indicate amino acids involved. Free energy corrections to account for constraints used to maintain complexes (see text) were found to be: a) 0.30±0.02 kcal/mol; b) −0.017±0.042 kcal/mol; c) −0.023±0.075 kcal/mol; d) 0.15±0.42 kcal/mol; and e) 0.34±0.12 kcal/mol. Uncorrected ΔΔG values are displayed within each panel after the specified transformations, with corrected ΔΔG values given at the top of each panel, corresponding to 1-ion, or 1st or 2nd ion of a 2-ion complex (with the cumulative 2-ion value indicated in parenthesis in panel c). Snapshots, with the DEKA ring in purple, EEDD ring in green, and the charged ammonium group of the Lys shown as blue and white balls, indicate starting configurations with Na^+ (orange balls) and K^+ (purple balls).

https://doi.org/10.1371/journal.pcbi.1006398.g010

the key energy controlling the different permeation mechanisms in Figs 7 and 9, but represents the relative stability of a complex that is particular to Na^+, and largely unseen for the K^+ ion because of its low stability, helping explain the distinct mechanisms.

During the ion crossing of the charged Lys, the ion creates a stable transition state together with the Lys and multiple carboxylates (Fig 10D; inset). This ion-Lys state is bound collectively by the D and E from the DEKA ring, as well as E_{II} from the outer ring, and shows preferential binding of a single Na^+ by 4.3±0.4 kcal/mol (Fig 10D). This ability to create a joint ion-Lys complex to facilitate crossing of the Lys in the S_{HFS} is the salient difference in Na^+ and K^+ permeation mechanisms.

The K^+ ion instead usually resides alone in the SF and crosses the ammonium group of the Lys further down, (Fig 10E; inset), where the electrostatic fields arising from carboxylates in the upper SF is less attractive. If we examine the relative free energies of Na^+ and K^+ ions in this region of the SF near the Lys, where such crossing occurs for K^+, we calculate a similar but reduced value of 3.1±0.2 kcal/mol, still favoring Na^+ (Fig 10E). This value remains negative because the ion remains in contact with D and E side chains from the DEKA ring as it passes the Lys side chain. Theoretically, both K^+ and Na^+ should be able to translocate in this fashion when the Lys moves downward, but this was not observed for Na^+. We may understand this from the relative destabilization of Na^+ in this region relative to the selective multi-carboxylate complexes that form above it, making downward movement of Na^+ less likely.

We therefore hypothesize that selective permeation in $Na_v1.2$ arises from the distinct mechanisms (Lys-complex pass-by Na^+ permeation versus electrostatically Lys plugged K^+ permeation), which originates from the difference in stabilities of multi-ion and ion-Lys complexes in the high field strength region of the SF. Multi-ion/multi-carboxylate complexes have also been seen to be crucial for Na^+ permeation in the bacterial Na_vAb channel, where a preference for single Na^+ ions of -2.2±0.6 kcal/mol has been estimated [30]. In the bacterial channel, we also suggest that optimal conduction requires the greater occupancy of the 3-ion state which is achieved when the crystallographic E177-S178 H-bond is lost on 2 opposite monomers, allowing the S_{HFS} carboxylate groups to reach toward the center of the SF and coordinate 2 Na^+ ions concurrently. This two-Na^+/two-carboxylate complex offers additional stability, allowing those 2 ions to coexist in S_{HFS}, and we calculate the relative stability of Na^+ vs. K^+ in S_{HFS} to become -3.8±0.2 kcal/mol in Na_vAb. This observation suggests that Na^+ ions adopt a specific 3-ion arrangement with 2 ions at the level of S_{HFS}, that does not occur in simulations of K^+, which closely parallels our observations in the $Na_v1.2$ channel.

Conclusions

The ability to select for native ions while discriminating against other similar ions, is one of the key features of voltage gated ion channels. Ion conduction is a dynamic process that involves

conformational isomerizations of the residues of the SF, as well as cooperation between multiple ions, requiring long timescale simulations to extract the underlying energetic landscape. In the absence of a high-resolution structure of a mammalian channel to study selectivity and conduction at the molecular level, we designed a model of the human $Na_v1.2$ by patching the essential sequence of residues in and around the SF, including the key DEKA and EEDD rings, into the Na_vRh bacterial channel. This $Na_vRh/Na_v1.2$ channel relaxes into an asymmetrical configuration, where the DEKA and EEDD rings are highly flexible and cooperate to ensure efficient conduction and selectivity for Na^+ over K^+, in line with previous studies of bacterial Na_v channels where similar flexibility has been shown to be critical for ion conduction [29, 30].

The presence of a positively charged Lys in Na_v channels has long been a source of intrigue; being essential for selectivity, but its specific role unexplained. Previous computational studies of eukaryotic Na_v models point toward a passive, hindering role, where the Lys side chain needs to bind away from the middle of the pore lumen in order to allow conduction of Na^+ ions. We reveal a more intimate role for this residue, depending on its protonation state. When Lys is deprotonated (neutral), we observe a 2 to 3-ion occupancy in the SF where both 2- and 3-ion knock on conductions are common, facilitated by tight multi-ion/multi-carboxylate complexes that are made possible by the flexible side chains of the SF. When Lys is instead protonated (charged), we see reduction to 1 to 2-ion occupancy, due to the extra charge introduced by the ammonium group of the Lys. In fact, we see the Lys actively participating in the conduction mechanism with a role similar to that of a permeating ion. In the presence of K^+ ions, the conduction mechanism instead relies on single ion permeation, where multi-ion/multi-carboxylate complexes are less likely.

These multi-Na^+/multi-carboxylate complexes help attract Na^+ in to the SF of $Na_v1.2$, where binding deeper in the SF stabilizes the ions. Interestingly, the carboxylates involved in these key multi-Na^+/multi-carboxylate complexes generally include only one carboxylate from DEKA and one or two from the EEDD ring in the vestibular region, rather than both D and E from the DEKA ring. This observation is consistent with mutagenesis experiments showing the need for only one of the D and E from the DEKA ring, supporting the idea of involvement of the outer ring [19]. These Na^+ favorable complexes are more commonly bound collectively by D and E_{II}. Cysteine mutations of the residues in the EEDD ring show the greatest decrease in conduction when this domain II Glu (E_{II} in our model) is mutated [25, 41], consistent with our observation that this residue from the outer ring is particularly important.

In the case of charged Lys we see conduction that is possible with a singly occupied SF, however, the binding of a second Na^+ ion reduces the conduction barrier by creating an intermediate state that enables efficient multi-ion conduction. The second Na^+ ion helps to push the ion already in the SF and stabilize a state where the ammonium group of the Lys and the bottom ion are collectively bound by the carboxylates, allowing the ion to pass by the Lys into the cavity. The facilitating of inward conduction by the presence of an additional external Na^+ ion may explain the robust inward rectification of current in mammalian Na_v channels seen experimentally [1]. Even though more space for conduction can be created in the SF by the steric unplugging of the ammonium group of the Lys, no conduction occurs in that state. This behavior is consistent and comparable with previous results in Na_vAb, where pass by of ion by another would only occur at the level of S_{HFS}. When the charged ammonium group of Lys is in the $S_{HFS,}$ where the electrostatic potential is most negative, it creates a smooth electrostatic environment leading into the cavity, whereas when it is in the down state it creates a zone of high electrostatic potential that cuts the cavity off from the SF. The Na^+ ion can benefit from the smooth energetic surface by binding at S_{HFS} in a multi-ion complex with Lys, whereas K^+ cannot; instead becoming partially electrostatically blocked by the Lys in the lower SF. This

illustrates the fundamental role of the Lys as an active participant in the selective conduction mechanism. K^+ is far less likely to form these multi-ion/multi-carboxylate complexes; in particular, we see preferential binding of 8.3±0.1 kcal/mol for Na^+-Na^+ over K^+-K^+ in these complexes. Furthermore, K^+ does not form the stable multi-carboxylate/Lys state. In fact, the ion+Lys/multi-carboxylate cluster favors Na^+ over K^+ by 4.3±0.4 kcal/mol. The consequence of this difference in affinity is a completely different conduction mechanism for K^+, having to pass the ammonium group of Lys in the lower part of the SF, where the electrostatic environment is not as favorable. Interestingly, the apparently independent conduction pathways for Na^+ and K^+ ions could potentially explain absence of anomalous mole fraction effects in mammalian Na_v channels [53]. In the future, simulations of a model human Na_v channel in an open conformation, based on constrained-open Na_vAb or Na_vMs structures [9, 16, 27], could be used to explore the competition of Na^+ and K^+ ions under the driving force of a membrane potential.

It has been proposed that mammalian Na_vs select for Na^+ via a different mechanism to bacterial Na_vs, owing to their divergent S_{HFS} site forming residues (EEEE Vs DEKA) [18, 80]. While this appears to be the case based on our observations, we do see evidence for common features that may be central to Na^+ selectivity. Both bacterial and human channels make use of an efficient multi-ion process enabled by flexible carboxylates binding two Na^+ ions during ion knock on or pass by conduction events. The efficiency of this multi-ion mechanism is reliant on the formation of 2-Na^+/2-carboxylate complexes, whose thermodynamic stabilities are increased for Na^+ compared to K^+. Even though bacterial channels possess 4 carboxylates at the S_{HFS} site, only two are needed for high affinity binding [30]. Thus, the bacterial channel uses two of its four EEEE Glus, whereas the human channel uses carboxylates both from the DEKA and EEDD rings, leading to a Na^+ permeation process that closely resembles our observations in the model human channel. However, the Lys residue in the human DEKA signature participates in the multi-ion knock-on mechanism in ways that impose a unique ion discrimination process, perhaps explaining the higher level of ion selectivity in mammalian Na_vs [1]. We propose that this additional selectivity is achieved by establishing distinct permeation mechanisms for Na^+ and K^+ ions, where the Lys expedites Na^+ translocation through high field strength complex formation, while partially blocking the K^+ ion.

Supporting information

S1 Text. Supplementary methods for *Selective ion permeation involves complexation with carboxylates and lysine in a model human sodium channel.*
(PDF)

S1 Table. Summary of ion binding in the $Na_v1.2$ SF of the $Na_vRh/Na_v1.2$ channel. The first column defines which carboxylate(s) the ion(s) are bound to. Columns 2,3 and 4 show the tight 2-ion/multi-carboxylate clusters for the $Na_v1.2$ SF with deprotonated Lys^0 in NaCl, protonated Lys^+ in NaCl, and protonated Lys^+ in KCl solutions, respectively. Columns 5 and 6 show the tight ion+Lys/multi-carboxylate clusters with protonated Lys^+ in NaCl and KCl solutions, respectively. Clusters that occur less than 4% of the time are not shown. Most commonly, Na^+ is bound to D and/or E together with E_{II}, whereas K^+ is bound to the outer EEDD ring or singly bound to only the DEKA D side chain.
(TIFF)

S1 Fig. Structural alignments of Na_v channels. Alignments of model human $Na_v1.2$ (pink) cockroach Na_vPaS (purple) and eel $Na_v1.4$ (blue), showing DI and DIII on top and DII and DIV at the bottom. Panel a) shows the alignment according to the backbone of the SF and outer vestibule based on all four subunits, while b) shows alignment according to the SF and

vestibule subunit by subunit, revealing the similarity of the $Na_v1.2$ model to Na_vPaS and $EeNa_v1.4$ cryoEM structures. Side chains of Glu, Asp and Lys are indicated with sticks.
(TIF)

S2 Fig. Na^+ ions in the SF of bacterial Na_vAb. 2D free energy projections showing: a) 2-ion occupancy; and b & c) 3-ion occupancy (graphed for all three ions in b, and the top two ions in c); where z_1, z_2, and z_3 correspond to the z positions of the bottom, middle and top ions, respectively, and where z_{23} is the z position of the COM of the top two ions. When there are 2 ions in the SF, the ions are trapped and it is not until a third ion enters from above that we can observe either a knock on or pass by conduction. Snapshots, with the EEEE ring in purple, indicate the corresponding Na^+ ion (orange balls) movements. State labels include a subscript 2 or 3, representing the 2-ion or 3-ion mechanisms, respectively. Here the state label A has no subscript because A_2 and A_3 represent the same state, with same 2-ion configuration in the SF, but with approaching 3rd ion from bulk.
(TIF)

S3 Fig. Radial distribution functions. Distributions are shown for Na^+-Na^+ (a), K^+-K^+ (b), Na^+-carboxylate (c) and K^+-carboxylate (d). Multi-ion clusters defined by $\boldsymbol{r < 4.7}$ Å for Na^+ and $\boldsymbol{r < 5.5}$ Å for K^+, and carboxylate binding by $\boldsymbol{r < 3.8}$ Å for Na^+ and $\boldsymbol{r < 4.2}$ Å for K^+.
(TIF)

S4 Fig. RMSD for the grafted region of the channel (residue numbers 174–184). a) Na^+ with deprotonated Lys^0; b) Na^+ with protonated Lys^+; and c) K^+ with protonated Lys^+. Red dashed lines indicate the level of RMSD after the equilibration period. Late changes due to the onset of conduction, particularly for K^+, are discussed in the text.
(TIF)

S5 Fig. Time series of C_α vertical positions for $Na_v1.2$ DEKA and EEDD residues. a) Na^+ with deprotonated Lys^0; b) Na^+ with protonated Lys^+; and c) K^+ with protonated Lys^+.
(TIF)

S6 Fig. Mean backbone fluctuations. Fluctuations are shown for residues 178 to 184 in Na_vRh/$Na_v1.2$ (yellow) and Na_vAb (blue) for: a) the mean of the four subunits (where orientation was according to all 4 subunits); and b) each individual subunit (where orientation was according to the subunit of interest).
(TIF)

S7 Fig. Ion coordination inside the channel. Mean ion coordination numbers relative to bulk water in Na_vRh/$Na_v1.2$ for: a) Na^+ with deprotonated Lys^0; b) Na^+ with protonated Lys^+; and c) K^+ with protonated Lys^+. Bulk hydration numbers are 5.67±0.04 for Na^+, and 6.94±0.07 for K^+.
(TIF)

S8 Fig. Occupancy analysis in the channel with neutral Lys^0 (deprotonated K of DEKA). a) Distribution of Na^+ occupancy and dominant clusters representing complexes with: b) 1-ion occupancies; c) 2 ion occupancies; and d) 3 ion occupancies. In panels c and d, 'single' clusters include 1-ion/1-carboxylate complexes only, 'multi' clusters include 1-ion/multi-carboxylate complexes with a loosely associated second ion, and 'tight multi' clusters represent 2-ion/multi-carboxylate clusters where both ions are within an ion-ion cut off, defined from the radial distribution function $g(r)$ for ion-ion distance (see text). The channel range is defined by the region $-15<z<15$ Å.
(TIF)

S9 Fig. Ion occupancies for the $Na_vRh/Na_v1.2$ SF with charged Lys^+ (protonated K or DEKA). a) Distribution of ion occupancies. Panels b and c show dominant cluster conformations for: 1-ion (b) and 2 ion (c) occupancies, for Na^+ (orange) and K^+ (blue). See S8 Fig for definitions.
(TIF)

S10 Fig. Free energy convergence analysis in the $Na_vRh/Na_v1.2$ channel for Na^+ with deprotonated Lys^0. Panel a shows the convergence of 1D free energy for the ion across the channel, comparing time ranges specified in the legend. The free energy profile converges quickly in the outer vestibule and SF, but more slowly in the central cavity because it takes longer for ions to enter this part of the channel. Panels b-e show convergence of 2D free energy maps corresponding to Fig 4, for the last 2 μs of each simulation (left and right show time ranges 0–1 μs and 0–2 μs, respectively).
(TIF)

S11 Fig. Free energy convergence analysis in the $Na_vRh/Na_v1.2$ channel for Na^+ with protonated Lys^+. Panel a shows the convergence of 1D free energy for the ion across the channel, comparing time ranges specified in the legend. Panels b-e, show convergence of 2D maps corresponding to Figs 6 & 7 (left and right show time ranges 0–3 μs and 0–4 μs, respectively).
(TIF)

S12 Fig. Free energy convergence analysis in the $Na_vRh/Na_v1.2$ channel for K^+ with protonated Lys^+. Panel a shows the convergence of 1D free energy for the ion across the channel, comparing time ranges specified in the legend. Panels b-d show convergence of 2D maps, corresponding to Fig 9 (left and right show time ranges 0–3 μs and 0–4 μs, respectively).
(TIF)

S1 Movie. Sodium ion movement in the $Na_v1.2$ SF with neutral Lys^0. Sample trajectory revealing interactions of Na^+ ions with the $Na_v1.2$ SF, showing multi-ion complexes involving carboxylates from inner DEKA and outer EEDD rings, and knock-on and pass-by conduction events. Na^+ ions are shown as orange balls, lysine N atom as a blue ball, and side chains of DEKA and EEDD rings as purple and green sticks, respectively.
(MP4)

S2 Movie. Sodium ion movement in the $Na_v1.2$ SF with charged Lys^+. Sample trajectory revealing interactions of Na^+ ions with the $Na_v1.2$ SF, showing multi-ion complexes involving inner DEKA and outer EEDD rings, and complex formation with the lysine ammonium group, enabling pass-by conduction events. Representations as in S1 Movie.
(MP4)

S3 Movie. Potassium ion movement in the $Na_v1.2$ SF with charged Lys^+. Sample trajectory revealing interactions of K^+ ions with the $Na_v1.2$ SF, showing ion interactions with DEKA and EEDD rings, lack of multi-ion or lysine complex formation, and conduction events requiring unblocking of the SF by downward movement of the lysine ammonium group. Representations as in S1 Movie, with K^+ ions shown as purple balls.
(MP4)

Acknowledgments

The authors would like to thank Phuong T. Nguyen (UC Davis) for his assistance in using Rosetta to rebuild missing loops in our $Na_v1.2$ model.

Author Contributions

Conceptualization: Toby W. Allen.

Data curation: Emelie Flood.

Formal analysis: Emelie Flood.

Funding acquisition: Toby W. Allen.

Investigation: Emelie Flood, Céline Boiteux, Toby W. Allen.

Methodology: Emelie Flood, Céline Boiteux, Toby W. Allen.

Project administration: Toby W. Allen.

Resources: Toby W. Allen.

Supervision: Toby W. Allen.

Visualization: Emelie Flood.

Writing – original draft: Emelie Flood, Toby W. Allen.

Writing – review & editing: Emelie Flood, Céline Boiteux, Toby W. Allen.

References

1. Hille B. Ion channels of excitable membranes: Sinauer Sunderland, MA; 2001.
2. Catterall AW. Structure and function of voltage-gated ion channels. Annual review of biochemistry. 1995; 64(1):493–531.
3. Lossin C, Wang DW, Rhodes TH, Vanoye CG, George AL. Molecular basis of an inherited epilepsy. Neuron. 2002; 34(6):877–84. PMID: 12086636
4. Akopian AN, Souslova V, England S, Okuse K, Ogata N, Ure J, et al. The tetrodotoxin-resistant sodium channel SNS has a specialized function in pain pathways. Nature neuroscience. 1999; 2(6):541–8. https://doi.org/10.1038/9195 PMID: 10448219
5. England S, de Groot MJ. Subtype-selective targeting of voltage-gated sodium channels. British journal of pharmacology. 2009; 158(6):1413–25. https://doi.org/10.1111/j.1476-5381.2009.00437.x PMID: 19845672
6. Payandeh J, Scheuer T, Zheng N, Catterall WA. The crystal structure of a voltage-gated sodium channel. Nature. 2011; 475(7356):353–8. https://doi.org/10.1038/nature10238 PMID: 21743477
7. Zhang X, Ren W, DeCaen P, Yan C, Tao X, Tang L, et al. Crystal structure of an orthologue of the NaChBac voltage-gated sodium channel. Nature. 2012; 486(7401):130–4. https://doi.org/10.1038/nature11054 PMID: 22678295
8. Shaya D, Findeisen F, Abderemane-Ali F, Arrigoni C, Wong S, Nurva SR, et al. Structure of a prokaryotic sodium channel pore reveals essential gating elements and an outer ion binding site common to eukaryotic channels. Journal of molecular biology. 2014; 426(2):467–83. https://doi.org/10.1016/j.jmb.2013.10.010 PMID: 24120938
9. McCusker EC, Bagnéris C, Naylor CE, Cole AR, D'Avanzo N, Nichols CG, et al. Structure of a bacterial voltage-gated sodium channel pore reveals mechanisms of opening and closing. Nature communications. 2012; 3:1102–10. https://doi.org/10.1038/ncomms2077 PMID: 23033078
10. Sula A, Booker J, Ng LC, Naylor CE, DeCaen PG, Wallace B. The complete structure of an activated open sodium channel. Nature Communications. 2017; 8.
11. Shen H, Zhou Q, Pan X, Li Z, Wu J, Yan N. Structure of a eukaryotic voltage-gated sodium channel at near-atomic resolution. Science. 2017; 355(6328):eaal4326. https://doi.org/10.1126/science.aal4326 PMID: 28183995
12. Yan Z, Zhou Q, Wang L, Wu J, Zhao Y, Huang G, et al. Structure of the Nav1. 4-β1 Complex from Electric Eel. Cell. 2017; 170(3):470–82. e11. https://doi.org/10.1016/j.cell.2017.06.039 PMID: 28735751
13. Charalambous K, Wallace BA. NaChBac: the long lost sodium channel ancestor. Biochemistry. 2011; 50(32):6742–52. https://doi.org/10.1021/bi200942y PMID: 21770445
14. Lee S, Goodchild SJ, Ahern CA. Local anesthetic inhibition of a bacterial sodium channel. The Journal of general physiology. 2012; 139(6):507–16. https://doi.org/10.1085/jgp.201210779 PMID: 22641643

15. Pavlov E, Bladen C, Winkfein R, Diao C, Dhaliwal P, French RJ. The pore, not cytoplasmic domains, underlies inactivation in a prokaryotic sodium channel. Biophysical journal. 2005; 89(1):232–42. https://doi.org/10.1529/biophysj.104.056994 PMID: 15849254

16. Bagnéris C, DeCaen PG, Naylor CE, Pryde DC, Nobeli I, Clapham DE, et al. Prokaryotic NavMs channel as a structural and functional model for eukaryotic sodium channel antagonism. Proceedings of the National Academy of Sciences. 2014; 111(23):8428–33.

17. Ren D, Navarro B, Xu H, Yue L, Shi Q, Clapham DE. A prokaryotic voltage-gated sodium channel. Science. 2001; 294(5550):2372–5. https://doi.org/10.1126/science.1065635 PMID: 11743207

18. Finol-Urdaneta RK, Wang Y, Al-Sabi A, Zhao C, Noskov SY, French RJ. Sodium channel selectivity and conduction: Prokaryotes have devised their own molecular strategy. The Journal of general physiology. 2014; 143(2):157–71. https://doi.org/10.1085/jgp.201311037 PMID: 24420772

19. Favre I, Moczydlowski E, Schild L. On the structural basis for ionic selectivity among Na+, K+, and Ca2+ in the voltage-gated sodium channel. Biophysical journal. 1996; 71(6):3110–25. https://doi.org/10.1016/S0006-3495(96)79505-X PMID: 8968582

20. Yue L, Navarro B, Ren D, Ramos A, Clapham DE. The cation selectivity filter of the bacterial sodium channel, NaChBac. The Journal of general physiology. 2002; 120(6):845–53. https://doi.org/10.1085/jgp.20028699 PMID: 12451053

21. Heinemann SH, Terlau H. Calcium channel characteristics conferred on the sodium channel by single mutations. Nature. 1992; 356(6368):441–3. https://doi.org/10.1038/356441a0 PMID: 1313551

22. Frank HY, Catterall WA. Overview of the voltage-gated sodium channel family. Genome biology. 2003; 4(3):207–14. PMID: 12620097

23. Catterall WA, Perez-Reyes E, Snutch TP, Striessnig J. International Union of Pharmacology. XLVIII. Nomenclature and structure-function relationships of voltage-gated calcium channels. Pharmacological reviews. 2005; 57(4):411–25. https://doi.org/10.1124/pr.57.4.5 PMID: 16382099

24. Terlau H, Heinemann SH, Stühmer W, Pusch M, Conti F, Imoto K, et al. Mapping the site of block by tetrodotoxin and saxitoxin of sodium channel II. FEBS letters. 1991; 293(1–2):93–6. PMID: 1660007

25. Schlief T, Schönherr R, Imoto K, Heinemann SH. Pore properties of rat brain II sodium channels mutated in the selectivity filter domain. European biophysics journal. 1996; 25(2):75–91. PMID: 9035373

26. Tang L, El-Din TMG, Payandeh J, Martinez GQ, Heard TM, Scheuer T, et al. Structural basis for Ca2+ selectivity of a voltage-gated calcium channel. Nature. 2014; 505(7481):56–61. https://doi.org/10.1038/nature12775 PMID: 24270805

27. Lenaeus MJ, El-Din TMG, Ing C, Ramanadane K, Pomès R, Zheng N, et al. Structures of closed and open states of a voltage-gated sodium channel. Proceedings of the National Academy of Sciences. 2017; 114:3051–60.

28. Ulmschneider MB, Bagnéris C, McCusker EC, DeCaen PG, Delling M, Clapham DE, et al. Molecular dynamics of ion transport through the open conformation of a bacterial voltage-gated sodium channel. Proceedings of the National Academy of Sciences. 2013; 110(16):6364–9.

29. Chakrabarti N, Ing C, Payandeh J, Zheng N, Catterall WA, Pomès R. Catalysis of Na+ permeation in the bacterial sodium channel NaVAb. Proceedings of the National Academy of Sciences. 2013; 110(28):11331–6.

30. Boiteux C, Vorobyov I, Allen TW. Ion conduction and conformational flexibility of a bacterial voltage-gated sodium channel. Proceedings of the National Academy of Sciences. 2014; 111(9):3454–9.

31. Corry B, Thomas M. Mechanism of ion permeation and selectivity in a voltage gated sodium channel. Journal of the American Chemical Society. 2012; 134(3):1840–6. https://doi.org/10.1021/ja210020h PMID: 22191670

32. Carnevale V, Treptow W, Klein ML. Sodium Ion Binding Sites and Hydration in the Lumen of a Bacterial Ion Channel from Molecular Dynamics Simulations. Journal of Physical Chemistry Letters. 2011; 2(19):2504–8.

33. Stock L, Delemotte L, Carnevale V, Treptow W, Klein ML. Conduction in a biological sodium selective channel. J Phys Chem B. 2013; 117(14):3782–9. https://doi.org/10.1021/jp401403b PMID: 23452067

34. Zhang X, Xia M, Li Y, Liu H, Jiang X, Ren W, et al. Analysis of the selectivity filter of the voltage-gated sodium channel Na_vRh. Cell Res. 2013; 23(3):409–22. https://doi.org/10.1038/cr.2012.173 PMID: 23247626

35. Qiu H, Shen R, Guo W. Ion solvation and structural stability in a sodium channel investigated by molecular dynamics calculations. Biochim Biophys Acta. 2012; 1818(11):2529–35. https://doi.org/10.1016/j.bbamem.2012.06.003 PMID: 22699041

36. Furini S, Domene C. On conduction in a bacterial sodium channel. PLoS computational biology. 2012; 8(4):e1002476. https://doi.org/10.1371/journal.pcbi.1002476 PMID: 22496637

37. Payandeh J, Minor DL Jr. Bacterial Voltage-Gated Sodium Channels (BacNaVs) from the Soil, Sea, and Salt Lakes Enlighten Molecular Mechanisms of Electrical Signaling and Pharmacology in the Brain and Heart. Journal of Molecular Biology. 2015; 427(1):3–30. https://doi.org/10.1016/j.jmb.2014.08.010 PMID: 25158094

38. Naylor CE, Bagnéris C, DeCaen PG, Sula A, Scaglione A, Clapham DE, et al. Molecular basis of ion permeability in a voltage-gated sodium channel. The EMBO journal. 2016:e201593285.

39. Ke S, Timin EN, Stary-Weinzinger A. Different inward and outward conduction mechanisms in NaVMs suggested by molecular dynamics simulations. PLoS Comput Biol. 2014; 10(7):e1003746. https://doi.org/10.1371/journal.pcbi.1003746 PMID: 25079564

40. Chiamvimonvat N, Perez-Garcia MT, Tomaselli GF, Marban E. Control of ion flux and selectivity by negatively charged residues in the outer mouth of rat sodium channels. The Journal of physiology. 1996; 491(1):51–9.

41. Chiamvimonvat N, Pé MT, Ranjan R, Marban E, Tomaselli GF. Depth asymmetries of the pore-lining segments of the Na+ channel revealed by cysteine mutagenesis. Neuron. 1996; 16(5):1037–47. PMID: 8630242

42. Tsushima RG, Li RA, Backx PH. P-loop flexibility in Na+ channel pores revealed by single-and double-cysteine replacements. The Journal of general physiology. 1997; 110(1):59–72. PMID: 9234171

43. Xia M, Liu H, Li Y, Yan N, Gong H. The mechanism of Na+/K+ selectivity in mammalian voltage-gated sodium channels based on molecular dynamics simulation. Biophysical journal. 2013; 104(11):2401–9. https://doi.org/10.1016/j.bpj.2013.04.035 PMID: 23746512

44. Li Y, Liu H, Xia M, Gong H. Lysine and the Na+/K+ Selectivity in Mammalian Voltage-Gated Sodium Channels. PloS one. 2016; 11(9):e0162413. https://doi.org/10.1371/journal.pone.0162413 PMID: 27584582

45. Mahdavi S, Kuyucak S. Mechanism of ion permeation in mammalian voltage-gated sodium channels. PloS one. 2015; 10(8):e0133000. https://doi.org/10.1371/journal.pone.0133000 PMID: 26274802

46. Noda M, Suzuki H, Numa S, Stühmer W. A single point mutation confers tetrodotoxin and saxitoxin insensitivity on the sodium channel II. FEBS letters. 1989; 259(1):213–6. PMID: 2557243

47. Khan A, Romantseva L, Lam A, Lipkind G, Fozzard H. Role of outer ring carboxylates of the rat skeletal muscle sodium channel pore in proton block. The Journal of physiology. 2002; 543(1):71–84.

48. Tsushima RG, Li RA, Backx PH. Altered ionic selectivity of the sodium channel revealed by cysteine mutations within the pore. The Journal of general physiology. 1997; 109(4):463–75. PMID: 9101405

49. Penzotti JL, Fozzard HA, Lipkind GM, Dudley SC. Differences in saxitoxin and tetrodotoxin binding revealed by mutagenesis of the Na+ channel outer vestibule. Biophysical journal. 1998; 75(6):2647–57. https://doi.org/10.1016/S0006-3495(98)77710-0 PMID: 9826589

50. Begenisich T, Cahalan M. Sodium channel permeation in squid axons. I: Reversal potential experiments. The Journal of physiology. 1980; 307(1):217–42.

51. Begenisich T, Cahalan M. Sodium channel permeation in squid axons. II: Non-independence and current-voltage relations. The Journal of physiology. 1980; 307(1):243–57.

52. French R, Worley J, Wonderlin W, Kularatna AS, Krueger B. Ion permeation, divalent ion block, and chemical modification of single sodium channels. Description by single-and double-occupancy rate-theory models. The Journal of general physiology. 1994; 103(3):447–70. PMID: 8037798

53. Ravindran A, Kwiecinski H, Alvarez O, Eisenman G, Moczydlowski E. Modeling ion permeation through batrachotoxin-modified Na+ channels from rat skeletal muscle with a multi-ion pore. Biophysical journal. 1992; 61(2):494–508. https://doi.org/10.1016/S0006-3495(92)81854-4 PMID: 1312366

54. Rakowski RF, Gadsby DC, De Weer P. Single ion occupancy and steady-state gating of Na channels in squid giant axon. The Journal of general physiology. 2002; 119(3):235–50. https://doi.org/10.1085/jgp.20028500 PMID: 11865020

55. Begenisich T, Busath D. Sodium flux ratio in voltage-clamped squid giant axons. The Journal of general physiology. 1981; 77(5):489–502. PMID: 6262428

56. Eisenman G, Latorre R, Miller C. Multi-ion conduction and selectivity in the high-conductance Ca^{2+}-activated K^{+} channel from skeletal muscle. Biophys J. 1986; 50(6):1025–34. https://doi.org/10.1016/S0006-3495(86)83546-9 PMID: 2432947

57. Gillespie D, Giri J, Fill M. Reinterpreting the anomalous mole fraction effect: the ryanodine receptor case study. Biophysical journal. 2009; 97(8):2212–21. https://doi.org/10.1016/j.bpj.2009.08.009 PMID: 19843453

58. Gillespie D, Boda D. The anomalous mole fraction effect in calcium channels: a measure of preferential selectivity. Biophysical Journal. 2008; 95(6):2658–72. https://doi.org/10.1529/biophysj.107.127977 PMID: 18515379

59. Nonner W, Chen DP, Eisenberg B. Anomalous mole fraction effect, electrostatics, and binding in ionic channels. Biophysical Journal. 1998; 74(5):2327–34. https://doi.org/10.1016/S0006-3495(98)77942-1 PMID: 9591660

60. Hille B. The permeability of the sodium channel to organic cations in myelinated nerve. The Journal of general physiology. 1971; 58(6):599–619. PMID: 5315827

61. Dudev T, Lim C. Factors governing the Na+ vs K+ selectivity in sodium ion channels. Journal of the American Chemical Society. 2010; 132(7):2321–32. https://doi.org/10.1021/ja909280g PMID: 20108922

62. Roux B. Exploring the ion selectivity properties of a large number of simplified binding site models. Biophysical journal. 2010; 98(12):2877–85. https://doi.org/10.1016/j.bpj.2010.03.038 PMID: 20550900

63. Brooks BR, Bruccoleri RE, Olafson BD, States DJ, Swaminathan S, Karplus M. CHARMM: A program for macromolecular energy, minimization, and dynamics calculations. Journal of computational chemistry. 1983; 4(2):187–217.

64. Kanai R, Ogawa H, Vilsen B, Cornelius F, Toyoshima C. Crystal structure of a Na+-bound Na+, K +-ATPase preceding the E1P state. Nature. 2013; 502(7470):201. https://doi.org/10.1038/nature12578 PMID: 24089211

65. Combs SA, DeLuca SL, DeLuca SH, Lemmon GH, Nannemann DP, Nguyen ED, et al. Small-molecule ligand docking into comparative models with Rosetta. Nature protocols. 2013; 8(7):1277–98. https://doi.org/10.1038/nprot.2013.074 PMID: 23744289

66. Isom DG, Castañeda CA, Cannon BR. Large shifts in pKa values of lysine residues buried inside a protein. Proceedings of the National Academy of Sciences. 2011; 108(13):5260–5.

67. Cymes GD, Ni Y, Grosman C. Probing the structure and electrostatics of ion-channel pores one proton at a time. Nature. 2005; 438(7070):975–89. https://doi.org/10.1038/nature04293 PMID: 16355215

68. Domene C, Furini S. Effects of the Protonation States of the EEEE Motif of a Bacterial Na+-Channel on Conduction and Pore Structure. Biophysical Journal. 2014; 106(2):130a.

69. Klauda JB, Venable RM, Freites JA, O'Connor JW, Tobias DJ, Mondragon-Ramirez C, et al. Update of the CHARMM all-atom additive force field for lipids: validation on six lipid types. The journal of physical chemistry B. 2010; 114(23):7830–43.

70. Jorgensen WL, Chandrasekhar J, Madura JD, Impey RW, Klein ML. Comparison of simple potential functions for simulating liquid water. The Journal of chemical physics. 1983; 79(2):926–35.

71. Brooks BR, Brooks CL, MacKerell AD, Nilsson L, Petrella RJ, Roux B, et al. CHARMM: the biomolecular simulation program. Journal of computational chemistry. 2009; 30(10):1545–614. https://doi.org/10.1002/jcc.21287 PMID: 19444816

72. MacKerell AD Jr, Bashford D, Bellott M, Dunbrack RL Jr, Evanseck JD, Field MJ, et al. All-atom empirical potential for molecular modeling and dynamics studies of proteins†. The journal of physical chemistry B. 1998; 102(18):3586–616. https://doi.org/10.1021/jp973084f PMID: 24889800

73. Shaw DE, Dror RO, Salmon JK, Grossman J, Mackenzie KM, Bank JA, et al., editors. Millisecond-scale molecular dynamics simulations on Anton. High performance computing networking, storage and analysis, proceedings of the conference on; 2009: IEEE.

74. Shaw DE, Grossman J, Bank JA, Batson B, Butts JA, Chao JC, et al., editors. Anton 2: raising the bar for performance and programmability in a special-purpose molecular dynamics supercomputer. Proceedings of the international conference for high performance computing, networking, storage and analysis; 2014: IEEE Press.

75. MacKerell AD, Feig M, Brooks CL. Extending the treatment of backbone energetics in protein force fields: Limitations of gas-phase quantum mechanics in reproducing protein conformational distributions in molecular dynamics simulations. Journal of computational chemistry. 2004; 25(11):1400–15. https://doi.org/10.1002/jcc.20065 PMID: 15185334

76. Lynagh T, Flood E, Boiteux C, Wulf M, Komnatnyy VV, Colding JM, et al. A selectivity filter at the intracellular end of the acid-sensing ion channel pore. eLife. 2017; 6:e24630. https://doi.org/10.7554/eLife.24630 PMID: 28498103

77. Kollman P. Free energy calculations: applications to chemical and biochemical phenomena. Chemical reviews. 1993; 93(7):2395–417.

78. Eisenman G, Krasne S, editors. Further considerations on the ion selectivity of carrier molecules and membranes. IV International Biophysics Congress Symposium on Membrane Structure and Function, Moscow; 1973.

79. Dudev T, Lim C. Ion selectivity strategies of sodium channel selectivity filters. Accounts of chemical research. 2014; 47(12):3580–7. https://doi.org/10.1021/ar5002878 PMID: 25343535

80. Ahern CA, Payandeh J, Bosmans F, Chanda B. The hitchhiker's guide to the voltage-gated sodium channel galaxy. The Journal of general physiology. 2016; 147(1):1–24. https://doi.org/10.1085/jgp.201511492 PMID: 26712848

81. Waterhouse AM, Procter JB, Martin DM, Clamp M, Barton GJ. Jalview Version 2—a multiple sequence alignment editor and analysis workbench. Bioinformatics. 2009; 25(9):1189–91. https://doi.org/10.1093/bioinformatics/btp033 PMID: 19151095